A new twist in ABC transporter mediated multidrug resistance – Pdr5 is a drug/proton co-transporter

Manuel Wagner[1,*,†], Daniel Blum[2,†], Stefanie L. Raschka[1,†], Lea-Marie Nentwig[1], Christoph G. W. Gertzen[3,4], Minghao Chen[6,7], Christos Gatsogiannis[6,7], Andrzej Harris[5], Sander H. J. Smits[1,3], Richard Wagner[2,*], Lutz Schmitt[1,*]

[1]Institute of Biochemistry, Heinrich-Heine-Universität Düsseldorf, Universitätsstraße 1, 40225, Düsseldorf, Germany.

[2] Department of Life Sciences and Chemistry, Jacobs University Bremen, 28719 Bremen, Germany

[3] Center for Structural Studies Heinrich-Heine-Universität Düsseldorf, Universitätsstraße 1, 40225, Düsseldorf, Germany.

[4] Institute of Pharmaceutical and Medicinal Chemistry, Heinrich-Heine-Universität Düsseldorf, Universitätsstraße 1, 40225, Düsseldorf, Germany.

[5] Department of Biochemistry, University of Cambridge, Tennis Court Road, Cambridge, CB2 1QW, United Kingdom.

[6.]Institute for Medical Physics and Biophysics and Center for Soft Nanoscience, Westfälische Wilhelms Universität Münster, 48149 Münster, Germany

[7.]Department of Structural Biochemistry, Max Planck Institute of Molecular Physiology, 44227 Dortmund, Germany.

*present address: Medac GmbH; Theatherstraße 6, 22880 Wedel, Germany

[*] Corresponding authors.

Email: ri.wagner@jacobs-university.de or Lutz.Schmitt@hhu.de

[†] These authors contributed equally to this work

Abstract

The two major efflux pump systems are involved in multidrug resistance (MDR): (i) ATP binding cassette (ABC) transporters and (ii) secondary transporters. While the former use binding and hydrolysis of ATP to facilitate export of cytotoxic compounds, the latter utilize electrochemical gradients to expel their substrates. Pdr5 from *Saccharomyces cerevisiae* is a prominent member of eukaryotic ABC transporters that are involved in MDR and used as a frequently studied model system. Although investigated for decades, the underlying molecular mechanisms of transport and specificity remain elusive. Here, we provide electrophysiological data on reconstituted Pdr5 demonstrating that this MDR efflux pump does not only actively translocate its substrates across the lipid bilayer, but generates a proton motif force in the presence of Mg^{2+}-ATP and substrates by acting as a proton/drug co-transporter. Importantly, a strictly substrate dependent co-transport of protons was also observed in *in vitro* transport studies using Pdr5-enriched plasma membranes. Similar observations have not yet been reported for any other MDR efflux pump. We conclude from these results that the mechanism of MDR conferred by Pdr5 and likely other transporters is more complex than the sole extrusion of cytotoxic compounds and involves secondary coupled processes suitable to increase the effectiveness.

Keywords:

ABC transporter/electrophysiology/membrane protein/molecular mechanism/multidrug resistance

Introduction

The phenomenon of multidrug resistance (MDR) exists in all cells ranging from prokaryotes to higher eukaryotes and describes the ability to prevent the efficacy of a wide range of functionally and structurally different cytotoxic compounds. One of the major mechanisms that confer MDR is the overexpression of certain efflux pumps expelling these toxic compounds into the extracellular space (1). Two classes of transporters are involved: (1) ATP binding cassette (ABC) transporters that utilize the binding and hydrolysis of ATP to transport their substrates and (2) secondary transporters of the major facilitator superfamily (MFS) as well as the RND and MATE family that use an existing electrochemical gradient across the membrane in order to export these compounds (2-5). Although studied for decades, the molecular mechanisms underlying the resistance conferred by these membrane proteins remain elusive in most cases (6).

In general, membrane transporters and channels are characterized by a high level of substrate specificity. Therefore, the large variety of substrates of individual MDR transporters raises the question whether these MDR transporters directly transport such a broad variety of structurally unrelated compounds or whether their physiological role within the cellular membrane indirectly protects the cell against cytotoxic compounds (2, 7). For the well-characterized human MDR ABC transporter P-gp (MDR1 or ABCB1), it was demonstrated that cells expressing this protein have an altered cytosolic pH and membrane potential compared to cells lacking MDR1. Earlier, *in vivo* studies revealed that Cdr1, a major MDR ABC transporter from pathogenic *Candida albicans* and a close homologue of *S. cerevisiae* Pdr5, alters the extracellular pH (8). Similar to MDR1, studies reported alterations of the membrane environment through altered ion gradients by MDR efflux pumps. In a study of the isolated transmembrane domain of the bacterial multidrug transporter LmrA from *Lactococcus lactis*, it was demonstrated that the transporter still facilitates proton motive force (PMF) driven uptake of drugs in absence of the nucleotide binding domains (NBDs) (9). This finding was later confirmed for full-length LmrA, which, however, requires that the physiological PMF results in the uptake of drugs through this membrane protein (10). The complexity of ion translocation by ABC transporters becomes more evident, if two other studies regarding this protein are taken into consideration. The first one demonstrated that LmrA is an ethidium bromide - H^+ - Na^+ - Cl^- symporter, while more

93 recently it was shown that it can act as a $Hepes^+$ - H^+ - $Cl^-/2Na^+$ antiporter (11, 12).
94 Another study involving the ABC transporter MsbA reported the requirement of the PMF
95 for this membrane protein, as ATP hydrolysis alone was insufficient to drive substrate
96 translocation (13).
97 In our study, we used purified Pdr5, a long and intensively-studied member of the
98 MDR ABC transporter family and the major player of the pleiotropic drug resistance
99 (PDR) network of *S. cerevisiae* (14-18). Like other MDR ABC efflux pumps, *in vivo* and
100 *in vitro* studies with plasma membrane vesicles clearly established that Pdr5 confers
101 resistance towards a wide variety of hydrophobic compounds that are structurally
102 unrelated, as well as metabolites (15, 17, 19). Only recently it was possible to isolate
103 this transporter and purify it in an active state (20). Based on this possibility, we
104 reconstituted Pdr5 into planar lipid bilayers and provide *in vitro* data demonstrating that
105 Pdr5 actually co-transports drug/protons in a strictly ATP- and substrate-dependent
106 manner. These results were supported by *in* vitro transport studies using plasma
107 membranes highly enriched in Pdr5. Importantly, we show that contrary to LmrA or
108 MsbA, Pdr5 does not rely on the presence of a PMF as an energy source, rather
109 generates itself a PMF across the membrane in the presence of ATP and substrate.
110 We conclude that the substrate/ATP induced PMF by Pdr5 serves as a self-activation
111 representing a new mechanism of MDR .
112
113

Results

In vitro transport assay for Pdr5

In our efforts to reconstitute purified wild-type Pdr5 ($Pdr5_{WT}$) into synthetic liposomes and to establish an *in vitro* transport assay, we noticed robust ATPase activity comparable to the activity observed in detergent micelles (20). In plasma membrane preparations containing $Pdr5_{WT}$, a robust, real-time rhodamine 6G (R6G) transport assay is often used to study $Pdr5_{WT}$ (17, 18). This assay is schematically summarized in Figure 1A. Here, plasma membranes enriched in $Pdr5_{WT}$ likely present as inside-out vesicles, although the precise nature (sheets or vesicles) of the plasma membrane is unknown, are used. Incubation of plasma membrane vesicles enriched in $Pdr5_{WT}$ with R6G results in a nearly quantitative insertion of R6G into the bilayer, followed by a slower equilibration between inner and outer leaflets (indicated as "1" in Figure 1A). Addition of ATP ("2") to the Mg^{2+} containing buffer results in energization of $Pdr5_{WT}$ and pumping of R6G from the outer to the inner leaflet, which decreases the R6G fluorescence intensity (ΔF_i). Normally, a decrease on the order of 50- 80% is achieved, which is due to oligomer formation that are non-fluorescent (17, 21). As soon as the active, $Pdr5_{WT}$ mediated transport and the spontaneous back flip of R6G reach equilibrium, no macroscopic change in the fluorescence intensity is observed ("3"). Addition of, for example, EDTA ("4"), which complexes the cofactor Mg^{2+}, restores the R6G fluorescence to its initial value prior to the addition of ATP ("5" in Figure 1A).

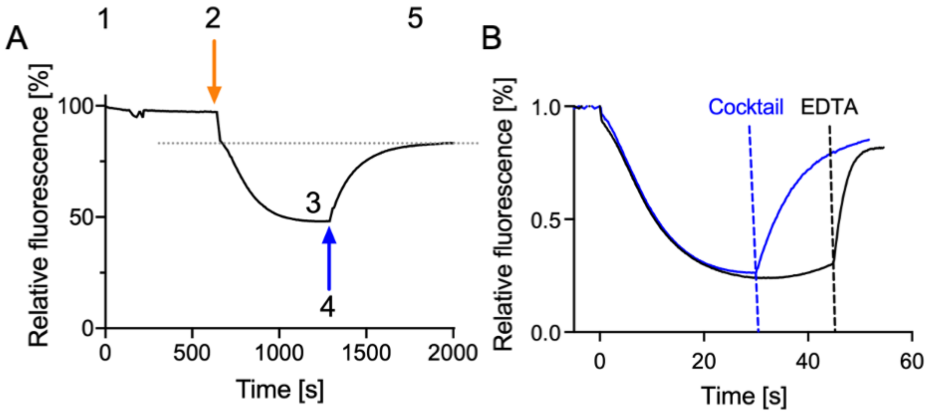

Figure 1. R6G transport assay. (A): Real-time R6G transport in Pdr5WT enriched plasma membranes. At time point 0, R6G is added to a solution containing yeast plasma membranes ("1"). After energization of $Pdr5_{WT}$ by addition of ATP ("2"), R6G is transported from the outer to the inner leaflet until a new equilibrium value of the fluorescence intensity is reached ("3"). The $Pdr5_{WT}$-mediated transport results in the

141 formation of non-fluorescent R6G oligomers in the inner leaflet as indicated by the
142 intensity drop of approximately 60%. At equilibrium, active transport of R6G by $Pdr5_{WT}$
143 and spontaneous flip-back reach steady state. At "4" the inhibitor EDTA, which
144 complexes the essential cofactor Mg^{2+}, is added, which results in restoration of the
145 initial fluorescence intensity ("5") which is highlight by the gray, dashed line. **(B):**
146 Dependence of R6G fluorescence intensity in plasma membrane preparations highly
147 enriched in $Pdr5_{WT}$ on ATP induced R6G transport in the absence (control) and the
148 presence of an artificial K^+ gradient. (Control): R6G transport was initiated by addition
149 of 5 mM ATP-Mg^{2+}, at the indicated time, EDTA (1 mM) was added. (K^+ gradient): After
150 addition of 100 mM KCl and 5 mM ATP-Mg^{2+}, nigericin (5 μM), valinomycin (0.18 μM)
151 and gramicidin (2 µg/ml) ("Cocktail") were added at the indicated time.
152
153 In contrast, in $Pdr5_{WT}$ containing proteoliposomes such a decrease was rarely
154 observed. Only in less than 10% of the attempts, ΔF_i as read-out for substrate transport
155 was detected with ΔF_i < 10%, not comparable to the more than 50- 80% decrease in
156 fluorescence intensity observed when employing plasma membrane preparations (17,
157 18). In light of the data available for LmrA and MsbA (11-13), we wondered whether ion
158 gradients might also have an impact on $Pdr5_{WT}$-mediated R6G transport. As a first step,
159 we prepared plasma membrane preparations enriched with $Pdr5_{WT}$ (18) and created
160 an artificial potassium and/or proton gradient by either adding 100 mM KCl and
161 valinomycin to the buffer (K^+ gradient). In the case of the K^+ gradient, R6G transport
162 was started by addition of 5 mM ATP/Mg^{2+} (Figure 1B). After the transport induced ΔF_i
163 reached a nearly steady state, EDTA was added to stop transport leading to nearly
164 complete reversal of ΔF_i. Next, we tested whether a complete short-circuit of the
165 membrane potential across the plasma membrane during the ATP/Mg^{2+} induced
166 transport might produce a similar effect on ΔF_i as EDTA before. For this, after the R6G
167 transport induced decrease of the fluorescence intensity reached a nearly steady state,
168 nigericin, valincomycin and gramicidin ("Cocktail") were added in low µM
169 concentrations to suppress the membrane potential completely (Figure 1B) (22, 23).
170 Remarkably, the short circuit of the membrane potential almost completely reversed
171 ΔF_i similar to EDTA (22). These results demonstrated that the fluorescence of R6G is
172 sensitive to electrochemical gradients (PMF) across the membrane. This confers with
173 the known sensitivity of R6G fluorescence towards pH (24) and the membrane potential
174 as derived from *in vivo* and *in vitro* studies (25-27). This also suggests that the decrease

175 in R6G fluorescence in plasma membrane preparation enriched in $Pdr5_{WT}$ might not
176 solely be due to formation of non-fluorescent dimers and trimers (21), but also to
177 changes in the membrane potential.

178 **$Pdr5_{WT}$ shows voltage dependent ion channel activity**

179 In order to verify whether $Pdr5_{WT}$ activity is modulated by an existing ion gradient
180 or may facilitate voltage activated ionic currents across a membrane, purified Pdr5 was
181 reconstituted into planar lipid bilayer (DOPC/DOPE, 7:3) and voltage dependent
182 currents across the bilayer were monitored. The high purity of the protein used in the
183 electrophysiological experiments was confirmed by MS analysis (see Table S1). In
184 addition to the control experiments with MOK-samples, the same data set as for $Pdr5_{WT}$
185 was also collected for the ATPase deficient E1036Q mutant (Pdr5EQ) (18).

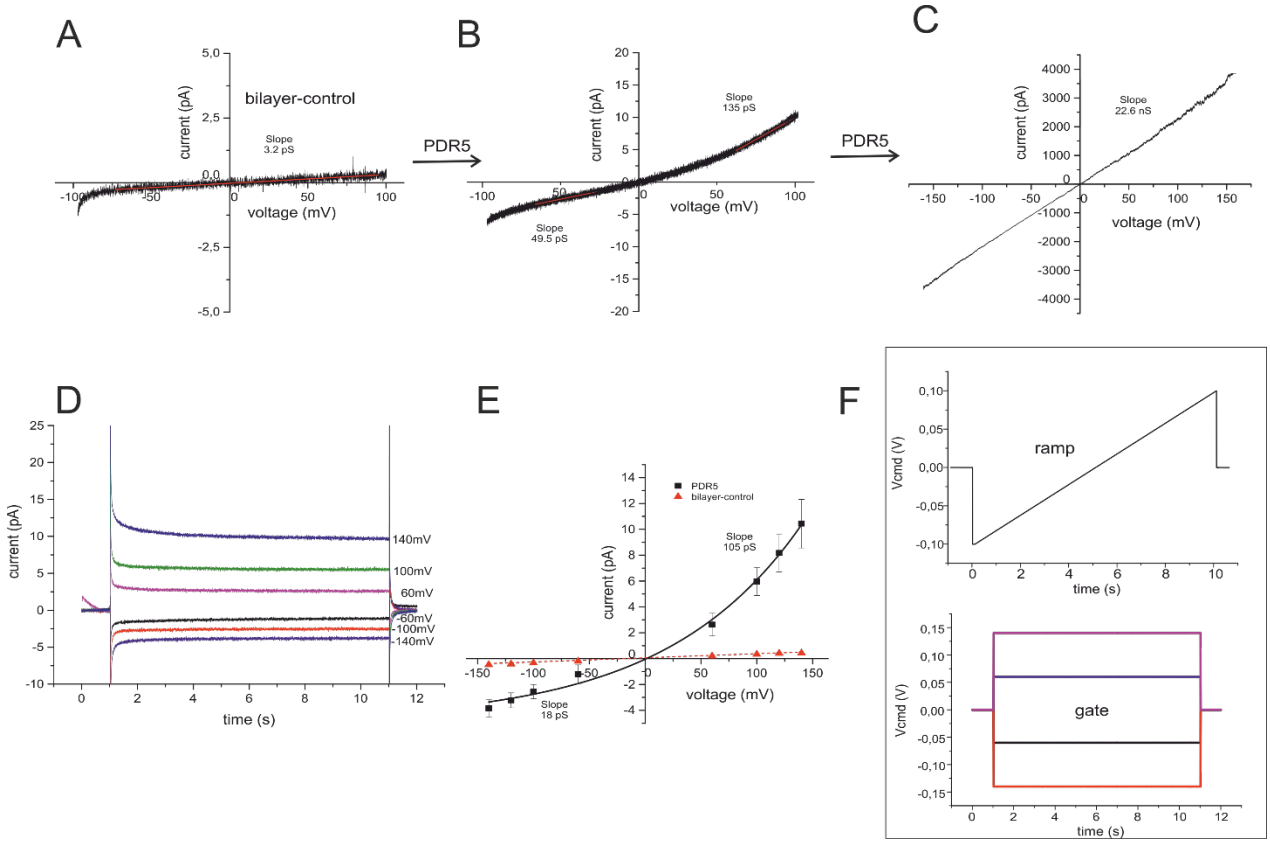

186
187

188 **Figure 2. Current recordings from a planar lipid bilayer containing**
189 **reconstituted $Pdr5_{WT}$.** (**A**) Current-voltage ramp measurement with a DOPE/DOPC
190 (7:3) bilayer in symmetrical cis/trans buffer conditions (250 mM KCl, 10 mM HEPES,
191 pH 7.0) (control). (**B**) Current recording of the same bilayer as in (**A**), but after insertion
192 of detergent purified $Pdr5_{WT}$ from the cis compartment using the voltage ramp protocol
193 shown in **(F)** (**C**) Current recording from a bilayer after multiple insertion of detergent

194 purified $Pdr5_{WT.}$ (**D**) Current-voltage gates of the same bilayer as in **(B)** using the
195 voltage gate protocol shown in F (lower part). **(E)** Current-voltage relation obtained from
196 the mean currents in **(D)**. (**F**) Applied voltage protocol for voltage- ramps (upper) and
197 voltage gates(lower).
198
199 The slope conductance of the control ("empty") bilayer was G_{sl} = 3.2 pS (Figure
200 2A) when a voltage ramp (V_h = -100 mV to +100 mV, see Figure 2F top) was applied
201 under symmetrical cis/trans conditions (250 mM KCl, 10 mM HEPES pH 7.0). However,
202 after addition of 2 μl detergent solubilized $Pdr5_{WT}$ (0.6 mg/ml) to the cis-compartment
203 with brief (2min) gentle stirring the voltage induced current across the bilayer increased
204 significantly and a slightly rectifying current voltage relation was observed (Figure 2B).
205 Addition of MOK samples did not show any effect on the i/v-curve. Moreover, repeated
206 aliquot addition (10 times) of the Pdr5 protein to the cis compartment resulted in a large
207 increase (~10^3-times) in the membrane currents as compared to the control (Figure
208 2C). Application of voltage gates on the same bilayer as in Figure 2B also showed a
209 significant increase of the membrane currents as compared to the control (Figure 2D)
210 and the resulting plot of the average current ($\bar{\imath}$) versus voltage (Figure 2E) resembled
211 closely the i/v- ramp in Figure 2B. These results give clear evidence that reconstituted
212 Pdr5 facilitates transport of K^+ and Cl^- ions at comparable high rates, which are also
213 dependent on the amount of reconstituted $Pdr5_{WT}$. Similar results have been obtained
214 for the ATPase deficient E1036Q mutant ($Pdr5_{EQ}$) (see below for details). In order to
215 check whether the high transport rates are caused either by a high number of copies
216 of active $Pdr5_{WT}$ in the membrane or by an "ion channel" mode, we have tested various
217 voltage protocols, which potentially could lead to ion-channel gating of $Pdr5_{W}$.
218 We could indeed find such a voltage-protocol (see Figure 3G, H). Starting from a
219 holding potential of V_h = +150 mV for 2-10 min. and using either voltage ramps (Figure
220 3G) or voltage gates (Figure 3H) we observed a significant increase of the $Pdr5_{WT}$-
221 mediated membrane currents accompanied by brief current flickering (Figure 3B) (G_{sl}
222 = 420pS,). Application of voltage gates allowed for a more detailed analysis of the
223 $Pdr5_{WT}$ mediated current gating (Figure 3C, D, E, F) and Figure S1). The graphs in
224 Figure 3 first clearly show that the reconstituted $Pdr5_{WT}$ mediates fast, flickering current
225 gating with different open channel amplitudes.

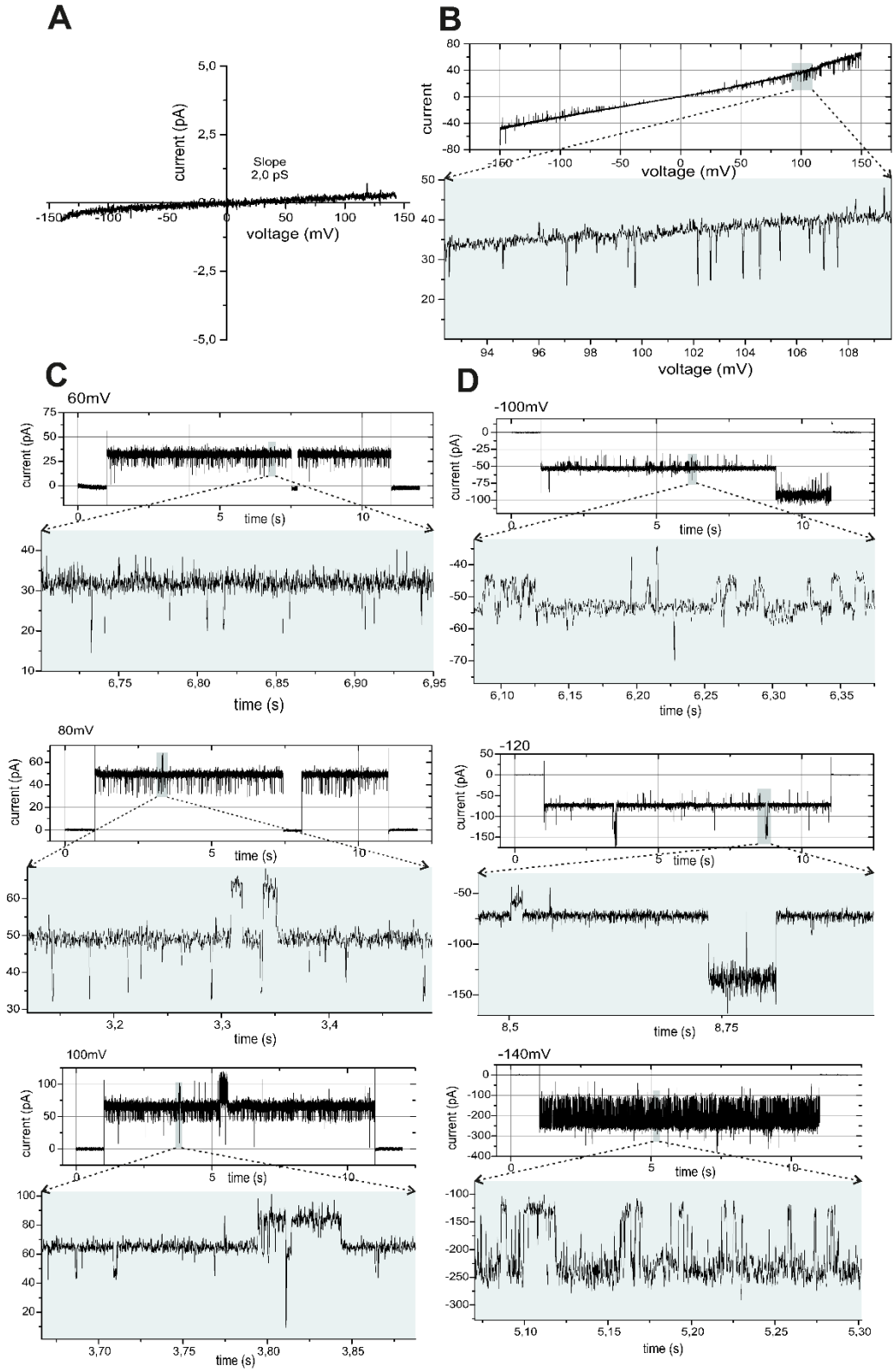
A
current (pA)
Slope
2,0 pS
voltage (mV)
B
current
voltage (mV)
voltage (mV)
C
60mV
current (pA)
time (s)
time (s)
80mV
current (pA)
time (s)
time (s)
100mV
current (pA)
time (s)
time (s)
D
-100mV
current (pA)
time (s)
time (s)
-120
current (pA)
time (s)
time (s)
-140mV
current (pA)
time (s)
time (s)

226

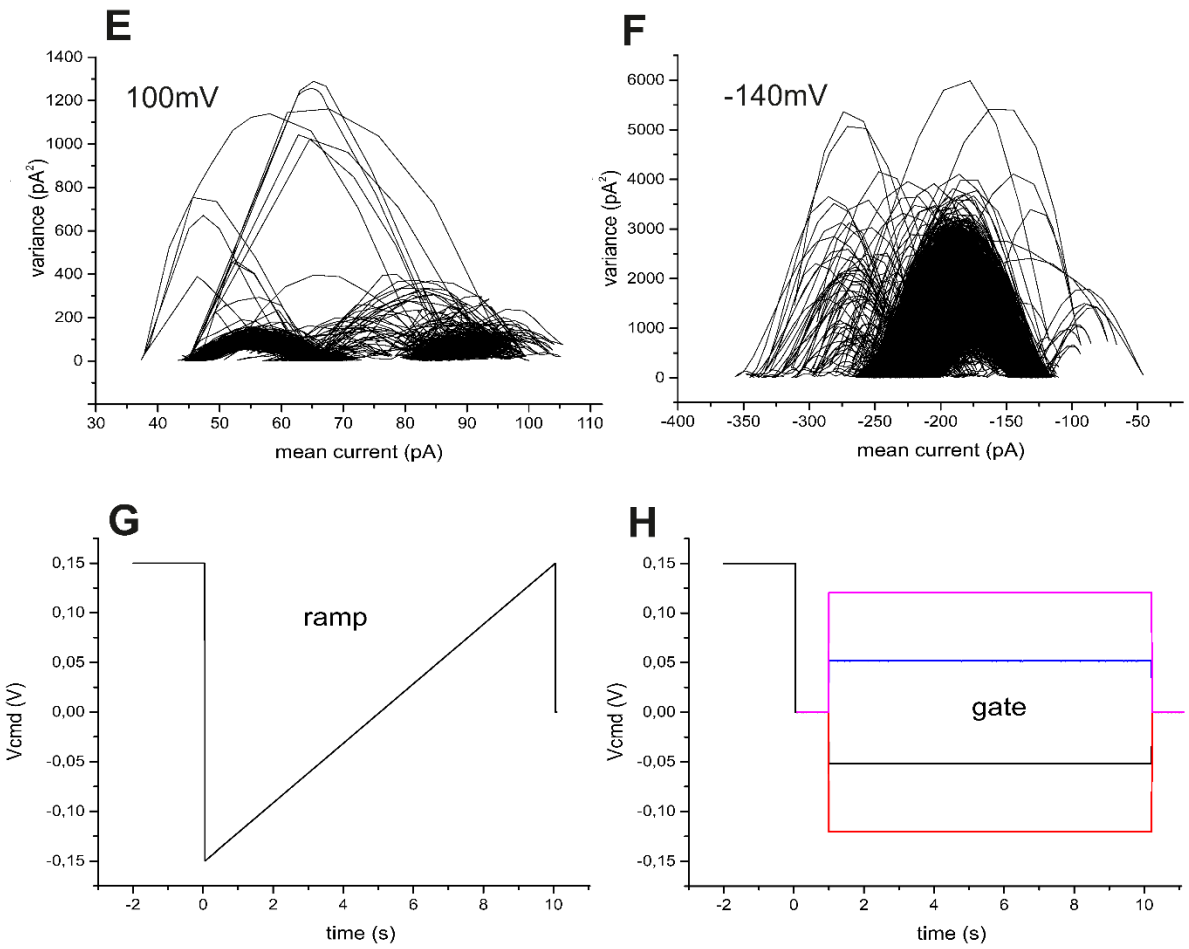

227

228

229 **Figure 3. Current recordings with extension plots from a bilayer containing**
230 **the reconstituted of Pdr5$_{WT}$**

231 **(A)** Current-voltage ramp measurement with a DOPE/DOPC (7:3) bilayer in
232 symmetrical cis/trans buffer conditions (control). (**B**) Current recording of the same
233 bilayer as in (**A**), but after insertion of detergent purified Pdr5$_{WT}$ from the cis
234 compartment using the voltage ramp protocol shown in **(G). (C), (D)** Extension plots of
235 current-voltage gates at the indicated V_h from the same bilayer as in **(B)** using the
236 voltage gate protocol given in **(H) (E), (F)** Mean variance plots for the respective
237 channel recordings shown in **(C)** and **(D)** depicting multiple open channel amplitudes.

238

239 Additionally, as indicated by the reproducible rectifying current-voltage relation,
240 Pdr5 incorporation into the membrane occurred almost exclusively unidirectional with
241 the nucleotide binding sites at the cis compartment (for more details see below).

242

243

244 **$Pdr5_{WT}$ possesses three main conductance states**

245 The analysis of the representative current recordings shown in Figure 3, with
246 voltage gates from V_h = ±60 mV to V_h = ±140 mV show that the observed complex
247 current gating pattern originates from one active channel with up to three open channel
248 amplitudes and not from simultaneous gating of multiple channels (see mean variance
249 analysis in Figure 3E, F and Figure S1). This conclusion is proven by looking closer
250 onto the combined current histogram and mean variance analysis of the current
251 recordings in Figure 3D at V_{cmd} = -140 mV indicating that channel gating occurred with
252 at least 3 different main open channel amplitudes. From the analysis of current
253 recordings at different membrane potentials (V_h =±60 mV to V_h =±140 mV, see Figure
254 2C) we collected from 5 different bilayer in a total of 40 recordings all point amplitude
255 histograms (Figure S1). The obtained currents at the given voltages were transformed
256 into conductance values binned in a histogram and the appearing peaks plotted in a
257 box-chart plot (Figure S1C). The following main mean conductance states of $Pdr5_{WT}$
258 were obtained: $G_1 \cong 55 \pm 24$ pS, $G_2 \cong 304 \pm 106$ pS, and $G_3 \cong 665 \pm 127$ pS. Closer
259 inspection of the time-course of gating events (see Figure 2C and Figure 2D) clearly
260 indicate that one single $Pdr5_{WT}$ unit displayed at least three distinct main
261 subconductance states (for more details see Methods in SI). The selectivity of the
262 $Pdr5_{WT}$ mediated ion currents was tested using asymmetric cis/trans buffer conditions
263 (see Figure S2) and gave a value of $P_{K^+}: P_{Cl^-} = 2.6: 1$.

264 Remarkably, the mean open state G_2 was mostly occupied at membrane
265 potentials above $V_{cmd} > \pm$ 100 mV. At an ionic strength of 250 mM and using the
266 simplified model of a cylindrical restriction channel region (28, 29) with a length of 1 nm,
267 we calculate from this conductance state the pore diameter of Pdr5 to be $d_{restriction} \cong 6.4$
268 Å.

269

270 **ATPase deficient E1036Q mutant ($Pdr5_{EQ}$) reveals similar properties as $Pdr5_{WT}$**

271 After addition of 1 µl detergent solubilized $Pdr5_{EQ}$ (2.0mg/ml) to the cis-
272 compartment with brief (2min) gentle stirring again voltage (voltage ramp starting at V_h
273 = 0 mV, see Figure 2F top) induced currents across the bilayer were observed. The
274 amplitude of the open channel currents appeared somewhat smaller as compared to

the Pdr5$_{WT}$ with slope conductance of G_{sl} =150 pS (-V$_{cmd}$) and G_{sl} =280 pS (+V$_{cmd}$) were observed (Figure 4A). Again, addition of MOK-samples did not show any effect on the control i/v-curve. Repeated addition (3-times) of the Pdr5 protein to the cis compartment resulted in a large increase (~5-times) in the membrane currents as compared to the control (Figure 4D). Application of voltage gates on the same bilayer as in Figure 4D also showed a significant increase of the membrane currents and the resulting plot of the average current ($\bar{\imath}$) versus voltage (Figure 4E) resembled closely the i/v- ramp in Figure 4D. These results show that that reconstituted Pdr5$_{EQ}$ facilitates transport of K^+ and Cl^- ions at high rates which are also dependent on the amount of reconstituted Pdr5$_{EQ}$.

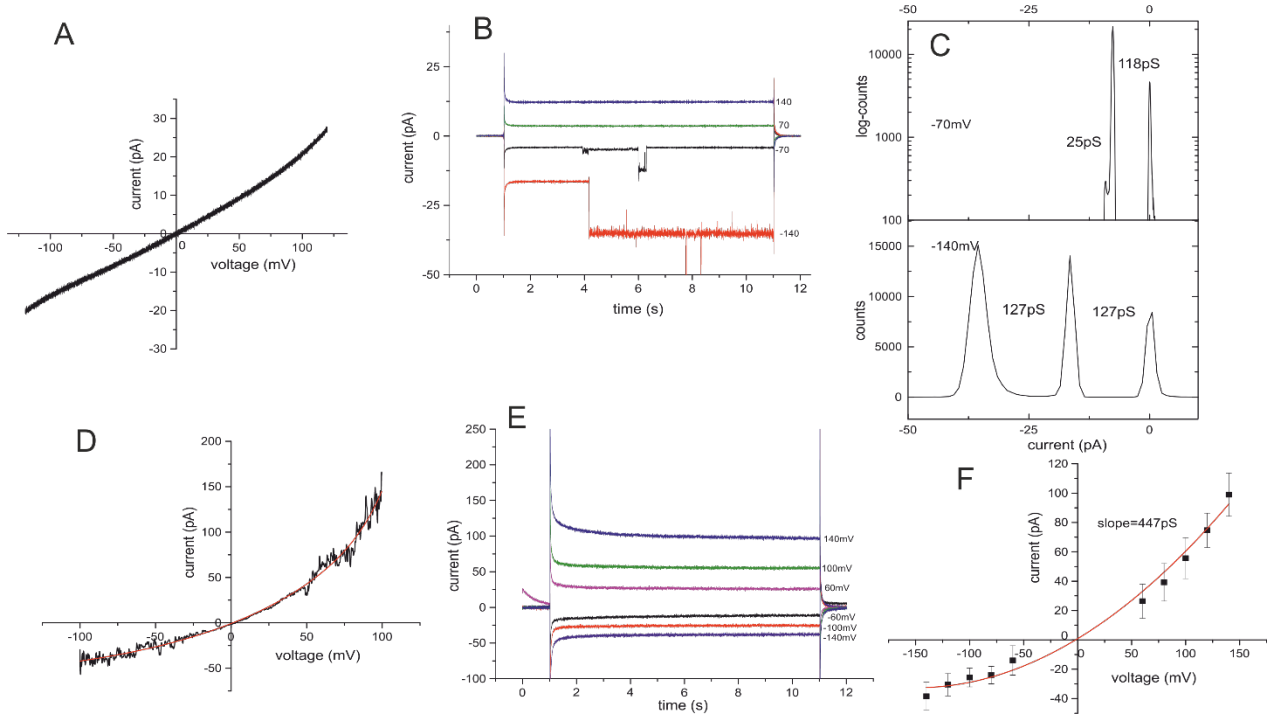

Figure 4. Current recordings from a bilayer containing the reconstituted of Pdr5$_{EQ}$. (**A**) Current-voltage ramp recording with a DOPE/DOPC (7:3) bilayer in symmetrical cis/trans buffer conditions after reconstitution of Pdr5$_{EQ}$ using the voltage ramp protocol shown in Figure 2F. (**B**) Current-voltage gates of the same bilayer as in **(B)** using the voltage gate protocol shown in F (lower part). **(C)** All point amplitude histograms for the recordings shown in **(B)**. **(D)** Current-voltage ramp recording with a DOPE/DOPC (7:3) bilayer in symmetrical cis/trans buffer conditions after multiple additions of Pdr5$_{EQ}$ to the cis compartment using the voltage ramp protocol shown in Figure 2F. (**E**) Current-voltage gates of the same bilayer as in **(D)** using the voltage

296 gate protocol shown in Figure 2F (lower part). **(F)** Current-voltage relation obtained
297 from the mean currents in **(E)**.
298
299 However, when the pre-activation command voltage protocol shown in Figure
300 3G,H was applied to the bilayer containing the reconstituted $Pdr5_{\mathbf{EQ}}$ rare current gating
301 events were only observed at negative V_{cmd} (Figure 4B). From a brief analysis of the
302 current gating events at V_{cmd} = -70 mV to -140 mV, the following main mean
303 conductance states of $Pdr5_{\mathbf{EQ}}$ were obtained: $G_1 \cong 35 \pm 12$ pS, $G_2 \cong 120 \pm 29$ pS. Thus,
304 the current gating properties of the $Pdr5_{WT}$ and the $Pdr5_{\mathbf{EQ}}$ mutant are different while
305 voltage activation of $Pdr5_{WT}$ leads to a strong current flickering mainly from the open to
306 the closed state the $Pdr5_{\mathbf{EQ}}$ mutant remains mainly in the open state with only low
307 frequent channel closures.
308 The ion selectivity of the $Pdr5_{EQ}$ mutant as determined in asymmetric cis/trans
309 buffer of $P_{K^+}: P_{Cl^-} = 3.5:1$ was close to the one of the $Pdr5_{WT}$ (see Figure S2).

310

311 **Modulation of Pdr5-mediated ion currents by its substrates**
312 We further tested the effect of known substrates namely R6G, ketoconazole (KA),
313 clotrimazole (CLO) and cycloheximide (CHX) on the voltage-induced ion channel
314 activity of $Pdr5_{WT}$.
315 Figure 5B shows a current-voltage ramp using the command-voltage protocol
316 shown in the inset of Figure 5A (control, empty bilayer) from a bilayer containing the
317 reconstituted $Pdr5_{WT}$ in symmetrical (cis/trans) buffer. As obvious, ion-conducting
318 activity with frequent channel gating was observed (see enlarged lower panel Figure
319 5B). The linear slope conductance indicated by the red line was G_{sl}= 525 ± 2.4 pS. This
320 value is very close to the $Pdr5_{WT}$ conductance state G_3 deduced from channel gating
321 (see above). Therefore, the current-voltage ramp can likely be attributed to a single
322 activated $Pdr5_{WT}$ unit. The brief flickering events resemble the respective channel
323 conductance G1 and G2 in their amplitudes. After addition of 2 mM Mg^{2+}-ATP
324 (cis/trans) and 330 nM R6G (1.2 μl 330 μM into 1.2 ml buffer) to the cis compartment
325 of the same bilayer no further voltage dependent channel gating could be observed
326 (Figure 5C). The current was drastically reduced while the form of the current-voltage
327 ramp changed to a more rectifying shape (Figure 5C). In addition, the zero-current

crossing (V_{rev}), changed completely and unexpectedly from V_{rev} = 0 mV to V_{rev} = -46 mV. This effect was reproducibly observed with an average V_{rev} = -43.8 ± 4.8 mV (n=7) no matter whether the bilayer contained single activated or multiple activated copies of $Pdr5_{WT}$. In this context, it is important to mention that this R6G-induced shift of V_{rev} was strictly dependent on the presence of Mg^{2+}-ATP in the cis compartment.

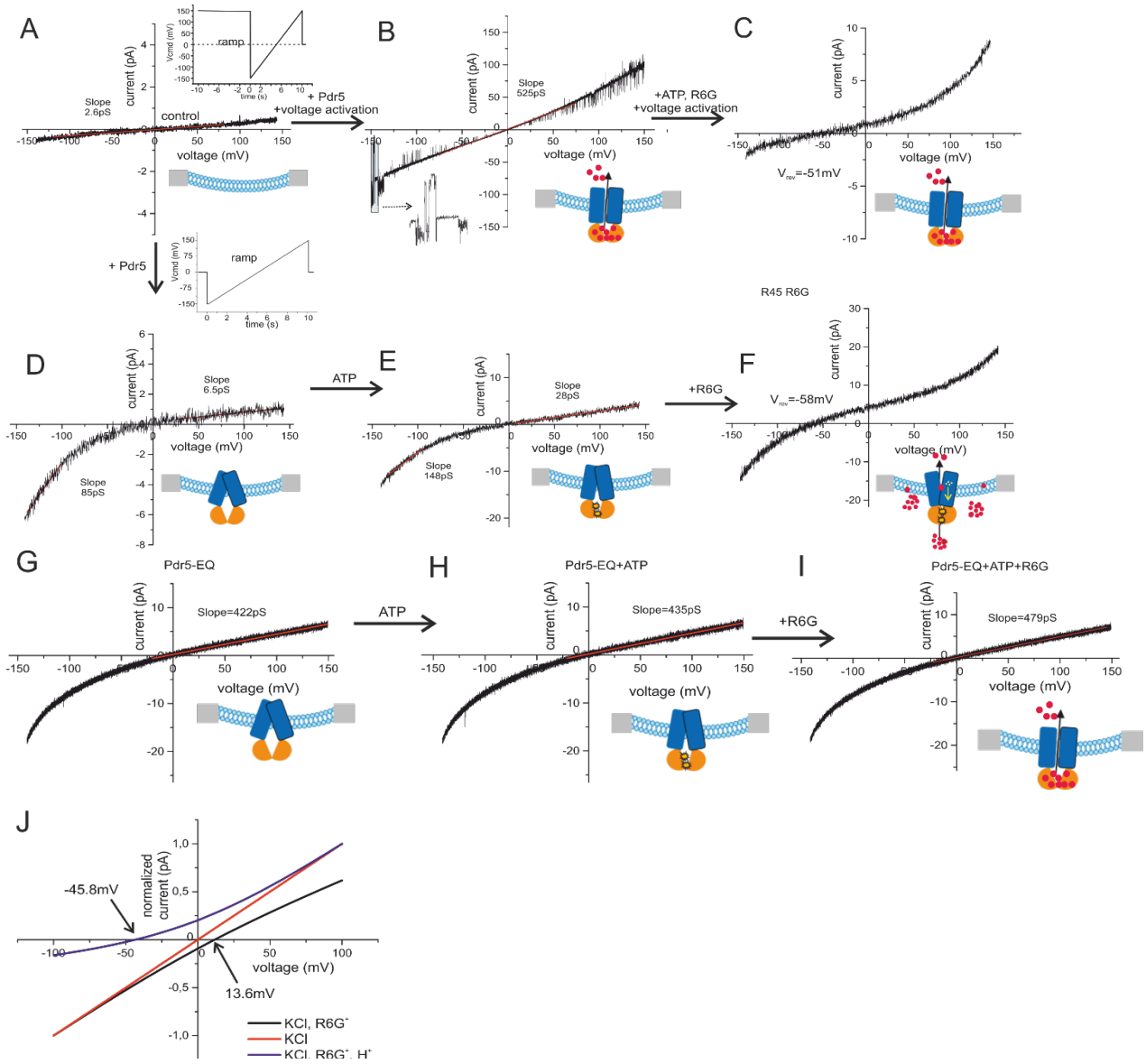

Figure 5. Effects of R6G on $Pdr5_{WT}$ and $Pdr5_{EQ}$ -mediated ion conductance. (**A**) Current-voltage ramp from an empty control bilayer under symmetrical buffer (cis/trans 250 mM KCl, 10 mM HEPES, pH 7.0) **(B)** Current-voltage ramp after reconstitution of $Pdr5_{WT}$ in symmetrical buffer using the command voltage protocol shown in the inset of **(A)**. **(C)** Same bilayer as in **(B)** but after addition (cis) of 1mM Mg^{2+}-ATP and 5µM R6G. (**D**) Current-voltage ramp in symmetrical buffer after reconstitution of $Pdr5_{WT}$ using the command voltage protocol shown in the inset below

342 **(A)**. Current-voltage ramp from the same bilayer as in **(D)** but after addition of 1mM
343 Mg^{2+}-ATP. **(F)** Same bilayer as in **(E)** but after addition of 5μM R6G. **(G)** Current-voltage
344 ramp in symmetrical buffer (250 mM KCl, 10 mM HEPES, pH 7.0) after reconstitution
345 of $Pdr5_{EQ}$ using the command voltage protocol shown in the inset below **(A)**. **(H)**
346 Current-voltage ramp from the same bilayer as in **(G)** but after addition of 1mM Mg^{2+}-
347 ATP (cis/trans). **(I)** Same bilayer as in **(H)** but after addition of 5μM R6G (cis). **(J)**
348 Current-voltage relations calculated by the GHK current equations using applied
349 experimental ionic conditions and the respective permeability ($P_{x,}$ $(P_{K^+}/P_{Cl^-}/P_{RG^+})$) as
350 variable (see supplemental Information for details) for 3 cases. **Red:** KCl (only
351 permeation of K^+ and Cl^- ions), **Black:** KCl-R6G (permeation of K^+ and Cl^- ions and
352 active transport of $R6G^+$ ions), **Blue:** KCl-R6G-H^+ (permeation of K^+ and Cl^- ions and
353 active co-transport of $R6G^+$ and H^+ ions). Currents were normalized to i_{max}. For more
354 details see Methods section and SI.
355
356 Addition of Mg^{2+}-AMP (trans) (n = 3) did not show this effect. Moreover, in this
357 setup of $Pdr5_{WT}$ reconstituted from the cis compartment, addition of the effectors to the
358 trans compartment (n=3) did also not show any effect. One may argue that the
359 observed shift might be generated due to electrode effects after the addition of 1.2μl
360 330μM R6G into 1.2ml buffer of the cis compartment only. However, this can be ruled
361 out from both theoretical and experimental considerations. We are using agar protected
362 Ag+/AgCl electrodes ($R_{typ} \cong 10k\Omega$), which are carefully checked for electrode offset
363 ($V_{typ}^{off} \leq 500\mu V$), which then is corrected automatically by the amplifier, at the beginning
364 of each bilayer recording (30). In none of the five control experiments with control
365 bilayers, the addition of 1.2 μl 330 μM R6G in EtOH had any effect on the electrode
366 potentials. Moreover, as outlined in more detail below no shift in V_{rev} was observed in
367 $Pdr5_{\mathbf{EQ}}$ containing bilayer at identical experimental conditions. The change in V_{rev} can
368 therefore only be due to an R6G induced trans-membrane flux of ions as source of the
369 additionally created membrane potential.
370 In order to explain the observed shift of V_{rev} the macroscopic GHK approach has
371 been widely used. This allows, -based on the ion composition in the cis and trans
372 compartments of the bilayer-, to calculate relative ion fluxes and zero current potentials.
373 Depending on the membrane permeability of the involved ions, the expected reversal
374 potentials for the flux of the given set of ions between the cis and trans compartment

375 separated by a selective permeable membrane can be calculated using the GHK
376 current equation ((31), the details can be found in SI).
377 The ion concentrations in the cis/trans compartments were kept symmetrical (250
378 mM KCl, 10 mM HEPES pH 7.0, 2 mM Mg^{2+}-ATP) before the addition of 330 nM R6G
379 to the cis compartment and we observed V_{rev} = 0 ± 1.5 mV (n=7). The calculation of the
380 expected V_{rev} by the GHK current equations (see SI for details) before and after addition
381 of charged R6G (charge=+1) clearly showed that the ion concentration at both sides of
382 the $Pdr5_{WT}$ containing membrane can by no means produce a current voltage-relation
383 with a zero-current crossing at V_{rev} = -43.8 ± 4.8 mV (see Figure S3). Therefore, we
384 must conclude that R6G induced a $Pdr5_{WT}$-mediated active ion transport of one of the
385 anions or cations present in solution. With symmetrical 250 mM KCl cis/trans, either Cl^-
386 ions would have to be transported from trans to cis to final concentrations of
387 $c_{trans}^{Cl^-} = 75\,mM\ and\ c_{cis}^{Cl^-} = 425\,mM$, or in the case of K^+ the ions would be transported
388 from cis to trans to final concentrations of $c_{cis}^{K^+} = 75\,mM$ and $c_{trans}^{K^+} = 425\,mM$ (for
389 details see SI). This massive ion pumping of one of the two ion species would in both
390 cases reduce (Cl^-) or increase (K^+) the bulk conductance value in either bilayer
391 compartments, which in fact was not observed. Consequently, transient flux of H^+ ions
392 is the remaining candidate to build up a membrane potential across the $Pdr5_{WT}$
393 containing bilayer yielding a zero-current potential of V_{rev} = -43.8 ± 4.8 mV. Introducing
394 H^+ as an additional ion in the macroscopic GHK current equations we can first
395 determine the direction of the H^+ flow in our experimental setup as well as the
396 hypothetical macroscopically related changes in the H^+ concentrations in the cis and
397 trans compartments. The GHK-calculations (details see SI) show that R6G transport is
398 accompanied by a H^+-transport from cis to trans.
399 Starting at pH 7 ($c_{cis/trans}^{H^+} = 100nM$) symmetrically, the calculated hypothetical
400 macroscopic changes of the H^+ concentrations in the cis and trans compartment yield
401 $c_{cis}^{H^+} = 7.94\,nM$ and $c_{trans}^{H^+} = 0.9\,\mu M$ (see Figure 5J and Figure S3 for calculation
402 details). However, since we detect ion flux induced membrane potentials generated by
403 a small number (n<< 100) of channels across a distance of ~20 nm (see SI for details),
404 which requires only tiny amounts of transported charges to establish the membrane
405 potential (see example calculation in SI for details), macroscopic changes of the H^+
406 concentrations would not be directly resolvable in our experimental setup.

As is obvious from the calculated current voltage relation with 2mM Mg^{2+}-ATP in cis/trans (Figure 5J), the observed shift of V_{rev} by R6G addition to the cis compartment in $Pdr5_{WT}$ containing bilayer could be explained by active H^+ transport (H^+ permeability $P_{H^+} \rightarrow \infty$) from the cis to the trans compartment. Calculation details for Figure 5J are given in SI.

In similar experiments, we tested whether the non-charged KA, CHX and CLO, other well-known substrates of $Pdr5_{WT}$, also modulate the activity of reconstituted $Pdr5_{WT}$ in planar bilayer. In a series of four different experiments, we observed a Mg^{2+}-ATP/KA induced shift of the zero-current potential of V_{rev} = -64 ± 8 mV (n = 4) (see Figure 6).

Based on these results, we conclude analogously that also KA in the presence of Mg^{2+}-ATP induces active $Pdr5_{WT}$-mediated H^+ transport from the cis to the trans compartment. Interestingly, with CHX as a potential substrate, we did not observe any significant modulation of $Pdr5_{WT}$-mediated currents, in contrast to R6G and KA. However, CLO (1 µM), when added to the cis compartment of a bilayer containing $Pdr5_{WT}$, induced a drastic shift of the reversal potential of V_{rev} = -57 ± 6.7 mV (n=4) in the presence of Mg^{2+}-ATP (cis) (see Figure 6).

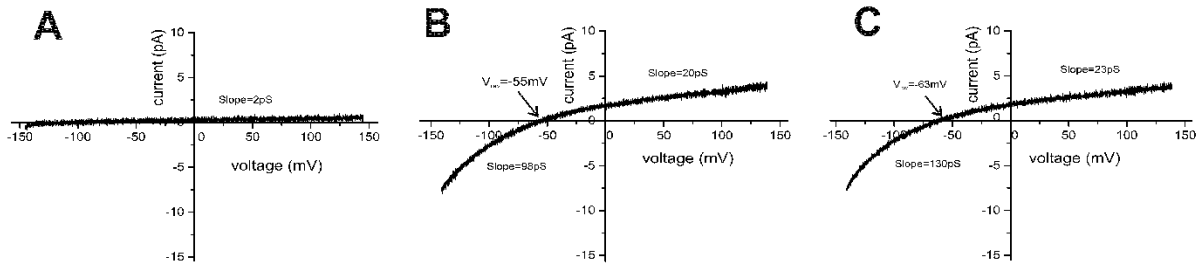

Figure 6. Effects of CLO and KA on Pdr5-mediated ion conductance. (**A**) Control bilayer after reconstitution of Pdr5. (**B**) Same bilayer as in (**A**) but after addition of 1µM CLO to the cis compartment. (**C**) Current-voltage recordings after addition of 330 nM KA to the cis compartment of a $Pdr5_{WT}$ containing bilayer.

The proton gradient is ATPase dependent

In order to verify the significance of the observed modulation of $Pdr5_{WT}$ activity by its substrates, we performed the same set of experiments as describe above except that we used the ATPase deficient $Pdr5_{EQ}$ mutant instead of $Pdr5_{WT}$. This therefore is

434 a proof whether the catalytic ATPase cycle is necessary for the observed shift of V_{rev}
435 and, most importantly, whether the observed ion currents are Pdr5-mediated. As shown
436 before in Figure 4 $Pdr5_{EQ}$ also incorporates into the planar bilayer membrane and
437 mediates voltage dependent ion currents across the membrane. However, $Pdr5_{EQ}$-
438 mediated currents were observed already at membrane potentials ≥ 20 mV. In more
439 than 90% of the attempts during voltage ramps rather large currents were observed
440 (Figure 4A,D) and correspondingly also in voltage gates (Figure 4E, F). These results
441 indicate that a high number of ion conducting $Pdr5_{EQ}$ have been incorporated into the
442 bilayer.
443 In addition, $Pdr5_{EQ}$ channel gating was rarely observed and the channels
444 remained almost exclusively in the open states as the determined conductance values
445 of the $Pdr5_{EQ}$ were in a similar range as for $Pdr5_{WT}$. This also holds true for the ion
446 selectivity of the $Pdr5_{EQ}$ mutant determined to be $P_{K^+}: P_{Cl^-} =$ =3.5:1 in comparison to
447 2.6:1 for $Pdr5_{WT}$ (see Figure S2 and SI for details). We also tested whether channel
448 currents of $Pdr5_{EQ}$ could be modulated by the substrates R6G and KA in a similar set
449 of experiments as described above for $Pdr5_{WT}$. We observed that in none out of the 15
450 attempts with R6G (see Figure 5G-I) or KA any modulation of $Pdr5_{EQ}$-mediated currents
451 showing that ATPase activity and transport of the substrate is an absolute requirement
452 for substrate induced change in V_{rev}.
453
454 **Beauvericin locks Pdr5 in an open state**
455 Beauvericin (BEA) is known as a potent inhibitor of Pdr5's ATPase and transport
456 activity (32) and additionally can mediate ion transport across the membrane most likely
457 in a carrier like mode (33). We therefore first investigated membrane currents after
458 addition of 0 µM, 3.3 µM and 9.9 µM BEA on the cis side (Figure 7A- C). The
459 conductance values of these measurements are listed in Table S3. Next, we addressed
460 the question whether BEA might suppress the substrate induced H^+ co-transport of
461 $Pdr5_{WT}$. Figure 7 D-G shows a representative series of experiments with an identical
462 bilayer. The graphs in Figure 7E demonstrates that $Pdr5_{WT}$ was incorporated in the
463 membrane and after addition of R6G to the cis compartment a shift of V_{rev} = - 51 mV
464 was observed. Remarkably, after addition of 1.65 µM BEA the overall current increased
465 significantly and the shift of the reversal potential disappeared completely (Figure 7G).

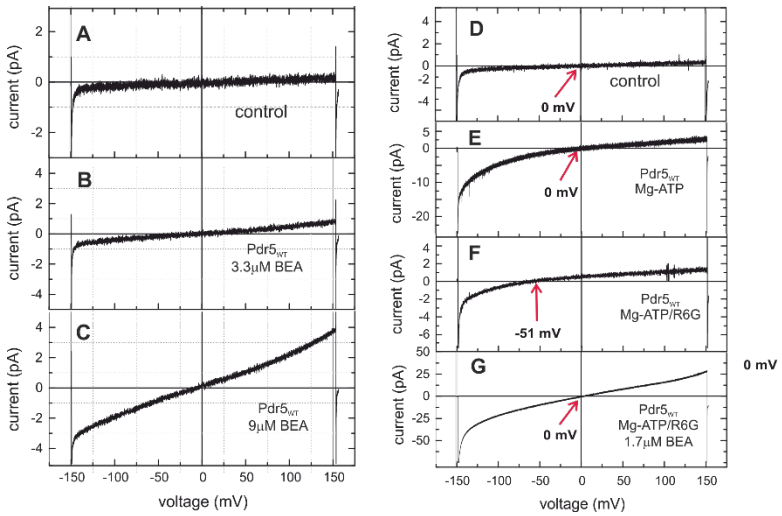

Figure 7. Current-Voltage recording in the presence of BEA in the cis compartment. (**A-C**) Current-voltage ramps with an empty bilayer (**A**) in the presence of 3.3 μM BEA, (**B**), 9.9 μM BEA and (**C**) 0 μM BEA, respectively. (**D-G**) series of current voltage ramps from a single bilayer: (**D**)**:** empty bilayer, (**E**) $Pdr5_{WT}$ incorporated in the presence of Mg^{2+}-ATP, (**F**) in the presence of Mg^{2+}-ATP/R6G and (**D**) is (**F**) after addition of 3.3 μM BEA.

The conductance values of the different measurements in Figure 7 D-G are listed in Table S4. These recordings show clearly that BEA can act as a carrier, but most importantly acts as a Pdr5 inhibitor that presumably locks Pdr5 in an open channel conformation.

Molecular docking suggests Beauvericin binding to the Pdr5 substrate binding site

Only recently, structural information of Pdr5 determined by single particle cryo EM became available (34). Thus, we used molecular docking to identify possible binding sites and states of BEA. The above described results suggest that BEA could bind to the R6G binding site to lock Pdr5 in an open state. However, as the starting conformation and placement of the ligand can have an influence on the results of the docking (35), although a small one, we used two different starting placements for BEA.

First, we placed BEA in the binding site of R6G (Figure 8A) as it is the most likely based on our experiments. Second, we placed BEA close to the transmembrane domains (TMDs) in the space between the TMDs and the nucleotide-binding domains (Figure 8B). The rational here was that due to its size BEA might bind to both TMDs

491 while allowing ion fluxes through its macrocycle as an alternative binding mode
492 hypothesis. To include receptor plasticity, we employed four different cryo-EM
493 structures of Pdr5 (34), which show different binding site conformations, after the
494 removal of ligands present in the respective structures. Scoring grids were calculated
495 for at least 40 Å around each initial BEA placements for each of the four Pdr5
496 conformations and subsequently both initial BEA conformations were docked into each
497 grid. This resulted in 16 valid suggested binding poses. Out of these 16 binding poses
498 nine bind to the R6G binding site in nearly identical conformations (Figure 8C)
499 regardless of their initial placement and center of docking grid. Here, BEA utilizes one
500 of its benzyl moieties such that it binds to a similar location as one of the benzene rings
501 of R6Gs xanthene-like moiety. The five binding poses not binding to the R6G binding
502 site of Pdr5 were either generated in the ADP-orthovanadate bound structure of Pdr5
503 (four poses) or R6G bound structure (one pose). The ADP-orthovanadate bound
504 structure of Pdr5 shows a shift of one of the transmembrane helices at the R6G binding
505 site. This shift renders the R6G binding site too narrow to accommodate BEA (Figure
506 8D). As a result, 90 % of all docked BEA binding poses in Pdr5 structures, which could
507 accommodate BEA in the R6G binding site, bind to exactly this binding site in nearly
508 identical conformations. This suggests that BEA binds to the R6G binding site in Pdr5.

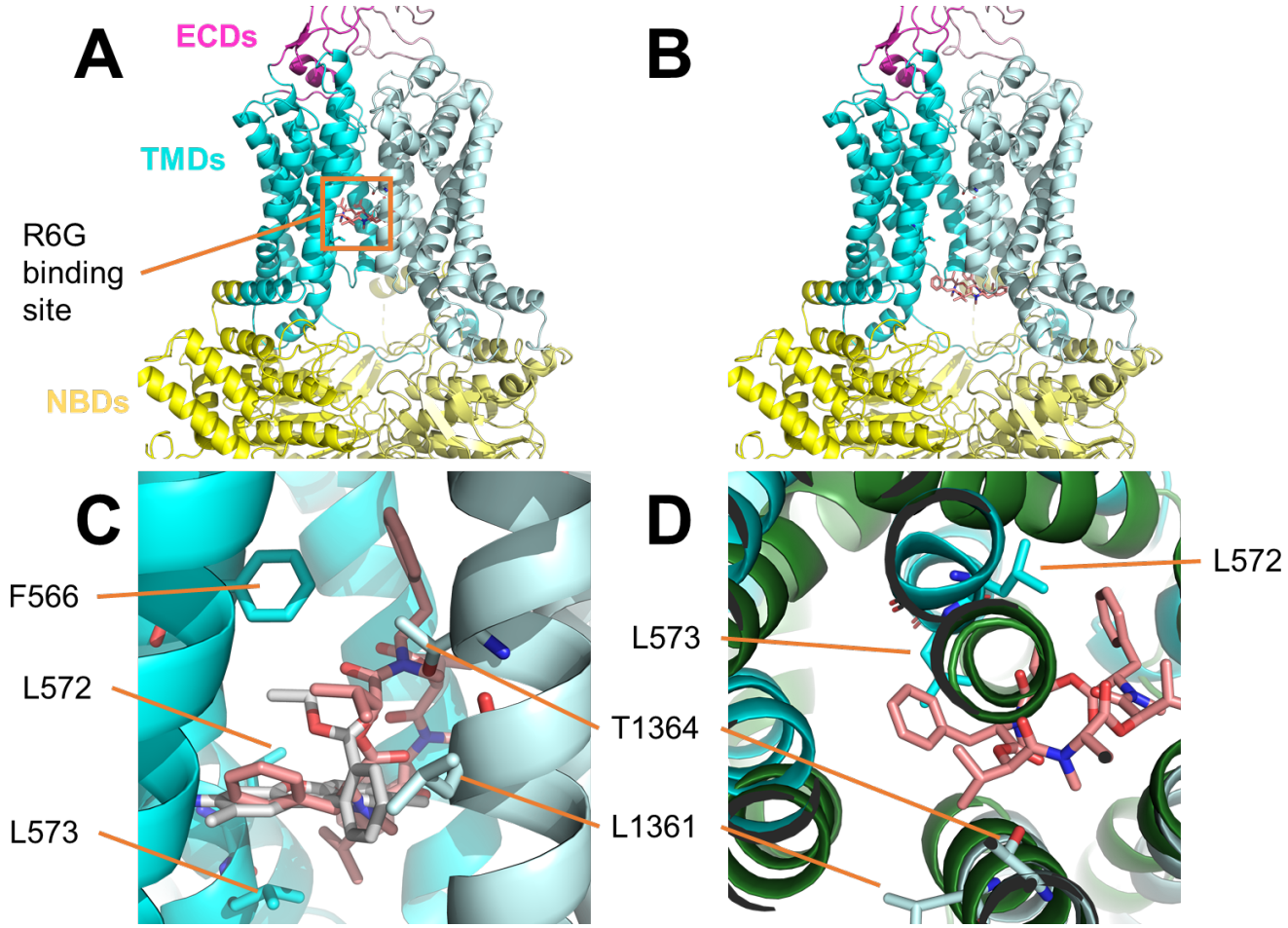

Figure 8. Suggested binding mode of beauvericin (BEA) in Pdr5 identified by molecular docking. (**A, B**) Initial placements and centers for the docking grid generation of BEA in the Rhodamin 6G (R6G) binding site (**A**) and between the TMDs and NBDs (**B**). BEA is shown in salmon sticks and the ectracellular domains (ECDs, magenta shades), transmembrane domains (TMDs, blue shades), and nucleotide binding domains (NBDs, yellow shades) of Pdr5 are shown as cartoon. The R6G binding site is indicated by an orange rectangle. Here the R6G bound structure of Pdr5 was chosen although R6G had been removed for docking and is thus not shown here. (**C**) Suggested binding mode of BEA in Pdr5, overlaid with the binding mode of R6G (white sticks) from the cryo-EM structure. Here, BEA places one of its benzyl moieties at a similar position as one of the benzene rings of R6Gs xanthene-like moiety. (**D**) Difference in the R6G binding site between the R6G and ADP-orthovanadate (AOV) bound Pdr5 structure (blue and green, respectively) viewed from above. The L572 and L573 containing helix in the AOV-bound structure moved towards the center of the R6G binding site and, thus, clashes with the suggested BEA binding mode. As a result, no

binding mode of BEA was identified int the R6G binding pocket of the AOV-bound structure during the docking.

In vitro measurement of substrate dependent H^+ co-transport

In order to verify the results of the electrophysiological single molecule experiments, we investigated the time-dependent change of the bulk pH value in suspensions with Pdr5 enriched plasma membrane vesicles under conditions of active Pdr5 substrate transport with a bulk fluorescence assay. Since many fluorophores are substrates of Pdr5WT, we used a pH sensitive fluorescein derivate (see SI for further details) conjugated to dextran with a molecular weight of about 40 kDa thus excluding that the dye might be a substrate of Pdr_{WT}. (17).

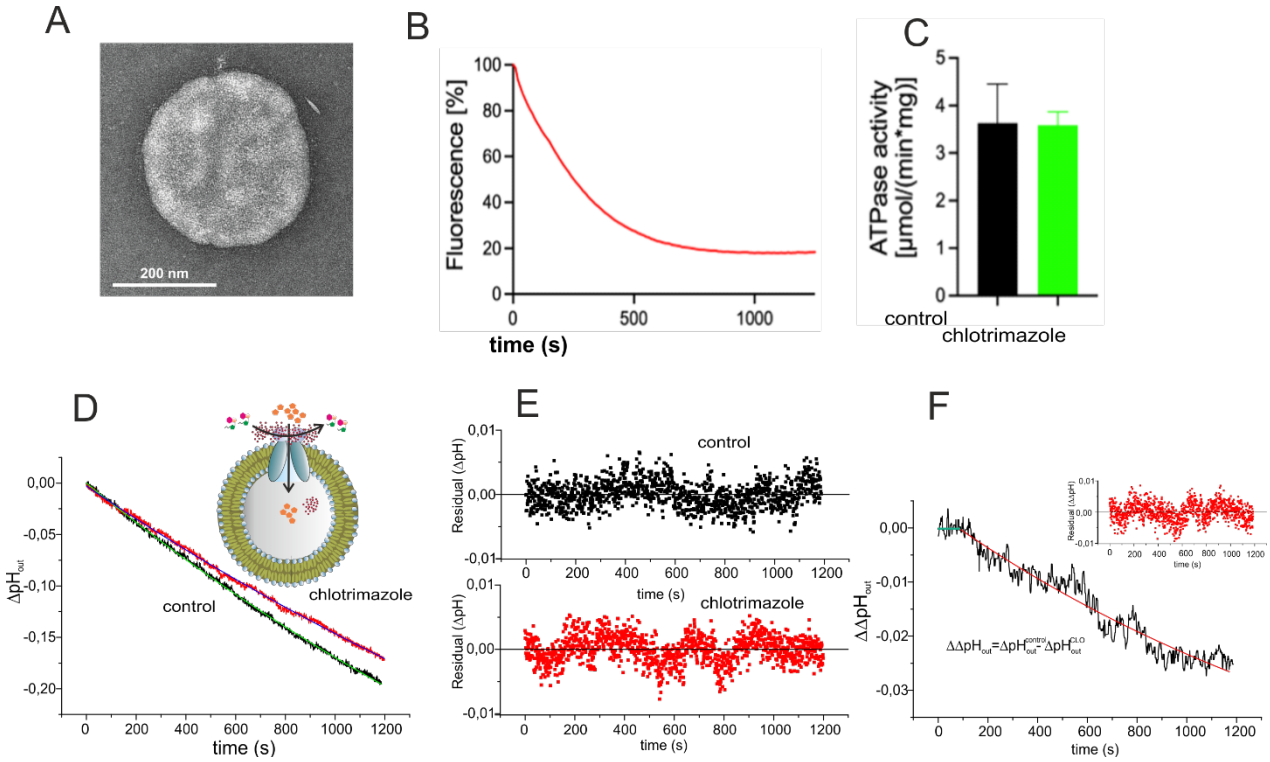

Figure 9. Fluorescence pH_{out} assay of ATP driven substrate transport in $Pdr5_{WT}$ in yeast plasma-membrane-vesicles. (**A**) A representative negative stain micrograph of yeast membrane-vesicles enriched with $Pdr5_{WT}$. Scale bar: 200 nm. **(B)** Control measument of R6G tranport in $Pdr5_{WT}$ yeast plasma-membrane-vesicles under identical experimental conditions of the pH_{out} measurements, i.e. without additional external buffer. (**C**) Monitor of the Pdr5-specific ATPase activity of the $Pdr5_{WT}$ membrane-vesicles under pH_{out} assy conditions in the absence (black bar) or in the

547 presence of 1 µM clotrimazole (green bar). Data represents the average of six
548 independent experiments with the error reporting the standrad deviation. p-value
549 determined by an unpaired t-test implemented in Prism 9 (GraphPad Inc.) between
550 both data sets is 0.859 indicating no significant differences in the respective ATPase
551 activity. (**D**) Time dependent pH_{out} changes monitored by dextran(40kD)-$fluorescein_{out}$
552 in the absence (control, black) or presence of 1 µM $clotrimazole_{out}$ (red).
553 Dextran(40kD)-fluorescein fluorescence was calibrated in the assay buffer containing
554 additional KP_i-buffer between pH6.5 and 8.0. For ease of visulaization, the time
555 dependent change of dextran(40kD)-$fluorescein_{out}$ fluorescence during the ATP
556 induced transport was -with the help of the calibration curve -converted directly into
557 ΔpH_{out} values and after averaging plotted as a function of time. Data represents the
558 average of three independent experiments with the error reporting the standrad
559 deviation. The solid lines (control, green; black, clotrimazole) represent the single
560 exponential decay fit of the respective experimental ΔpH_{out} decay curves. **(E)** Residuals
561 of the respective data-fit in (D). **(F)** Calculated difference ($\Delta\Delta pH_{out} = \Delta pH_{out}^{control} -$
562 ΔpH_{out}^{CLO}) of the time-dependent ΔpH_{out} changes. Solid line shows the single exponential
563 fit of the respective $\Delta\Delta pH_{out}$ curve and the inset the residuals of the fit.
564
565 Furthermore, we visualized Pdr5 enriched plasma membrane vesicles using negative
566 stain electron microsopy. Both yeast plasma membrane preparations of
567 $Pdr5_{WT}$ and $Pdr5_{EQ}$ form typical uniform vesicular structures with an average diameter
568 of 300-500 nm (Fig. 9A).
569 These figures show that the stable yeast plasma membrane vesicle preparations meet
570 the requirements to enable the investigation of bulk pH-changes mediated by
571 transporter induced vectorial flux of substrates between the bulk phase and the inner
572 lumenial space of the vesicles.
573 Second, we analyzed whether the low buffer capacity conditions required for the pH-
574 assay might effect or even abolish $Pdr5_{WT}$ mediated R6G transport in plasma
575 membrane vesicles. As shown in Figure 9C, quenching of R6G fluorescence as read-
576 out for Pdr5 transport activity was quantitatively not impaired and the ΔF_i-equilibrium
577 value reached approximately 20% residual fluorescence-intensity, which is well in the
578 range of published values (17, 18). For ΔpH_{out} measurements, CLO was selected as
579 substrate as it is at the given experimental conditions (in contrast to R6G) non-
580 fluorescent and showed a V_{rev} = -57 ± 6.7 mV in the single channel recordings (Figure

581 6). Third, we checked wether the Pdr5-specific ATPase activity of the Pdr5 enriched
582 membrane-vesicles under pH_{out} assay conditions were impaired in the presence of 1
583 µM clotrimazole outside. As shown in Figure 9D within error limits no differences
584 between the ATPase activity of the control (black) and the one in the presence of 1 µM
585 clotrimazole outside could be detected.
586 Furthermore we have recorded the time-dependent change of the bulk pH value
587 (ΔpH_{out}) in the suspension with Pdr5 enriched plasma membrane vesicles under
588 conditions of active Pdr5 substrate transport. We observed a time dependent decrease
589 of the dextran(40kD)-$Fluorescein_{out}$ fluorescence intensity (ΔpH_{out}). Three independent
590 sample-recordings but with identical assay conditions were averaged and the observed
591 time dependent fluorescence changes were with the aid of the calibration curve (see
592 Materials and Methods) -converted directly into ΔpH_{out} values and plotted as a function
593 of time. Figure 9E shows the timecourse of the ΔpH_{out} changes in the absence (black)
594 and the presence of 1 µM clotrimazole (red). The solid lines in the respective recordings
595 represent the results of the mono-exponential fit of the data and in Figure 9F the
596 respective residuals of the fit are shown. As already obvious from the raw graph there
597 is a significant difference in the time course of the decay curves. The fit of the single
598 exponential ΔpH_{out} decay revealed time constants of $\tau = 2147.8\ \mathrm{min}^{-1}$ (control) and
599 $\tau = 2699.7\mathrm{min}^{-1}$ (CLO). Thus the relative ATP hydrolysis related H^+-release per time-
600 unit as shown in the decay curve of the control due to the uncoupled ATPase activity
601 of $Pdr5_{WT}$ (18), which releases one proton per hydrolyzed ATP, is reduced by a factor
602 of 0.8 during CLO transport. Since however a CLO induced inhibition of ATPase
603 activity has been ruled out experimentally (Figure 9F) the apparent lower amount of
604 released H^+ can in light of the electrophysiological results conclusively be explained by
605 the substrate dependent co-transport of H^+. The time course of the difference of ΔpH_{out}
606 ($\Delta\Delta pH_{out} = \Delta pH_{out}^{control} - \Delta pH_{out}^{CLO}$) is shown in Figure 9G, the solid line represents the
607 single exponential fit with a decay rate of $\tau = 1350\ \mathrm{min}^{-1}$ and the inset the respective
608 residuals of the fit. Since we present strong evidence that this time dependent decrease
609 of pH_{out} represents the rate of H^+ cotransport into the vesicle lumen this results in an
610 overall rate of $\tau = 1350\ \mathrm{min}^{-1}$ for the H^+-co-transport by Pdr5 in the vesicle suspension.
611 In summary the results of the bulk fluorescence assay -which allowed us to determine
612 – bulk pH changes in suspensions with Pdr5 enriched plasma membrane vesicles
613 under conditions of active Pdr5 substrate transport- agree very well with the
614 electrophysiological single molecule results and show that Pdr5 is an H^+-cotransporter.

615

616 **Discussion**

617 MDR ABC transporters have a broad range of substrates that are highly diverse
618 in terms of structure and physico-chemical properties. There has been a long debate
619 on how these membrane proteins confer resistance, i.e. how transporters reduce the
620 drug concentration within a cell. Currently two models are favored: (i) the 'drug pump
621 model', in which ABC transporters actively expel the compounds out of the cell is
622 supported by numerous studies (36, 37) and (ii) the 'altered partitioning model', in which
623 MDR ABC transporters confer resistance by alteration of the membrane environment
624 through ion transport that ultimately results in lower drug uptake by the cell (7, 8, 12,
625 38). Essentially, the question arises whether all of the known substrates of MDR
626 transporters are actually real substrates in terms of being actively transported out of
627 the cell against the concentration gradient, or if these proteins mediate a decreased
628 influx of the drugs by altering membrane properties, or whether both mechanisms are
629 actually used.

630 With regard to these open questions, we tried to establish an *in vitro* transport
631 assay for the well-studied yeast MDR ABC transporter Pdr5 (for a recent review see
632 (16)). This transporter has been extensively studied in the last three decades and a
633 robust *in vivo* transport assay based on the Pdr5- and ATP/Mg^{2+}-dependent R6G
634 quenching in plasma membrane preparation is available (17, 18). Despite all our efforts,
635 we could not transfer the plasma membrane-based transport assay to proteoliposomes.
636 Nevertheless, we also detected that the R6G transport in plasma membrane
637 preparation was strongly dependent on artificial ion gradients (Figure 1), which is
638 supported by other studies (25-27). Therefore, we turned to an electrophysiological *in*
639 *vitro* approach, which enabled us to measure directly Pdr5-mediated ion conductivities
640 under varying conditions. Previously, studies performed on MsbA and LmrA
641 demonstrated that ion gradients benefit or are even indispensable for the activity of the
642 respective ABC transporter, while ATP, the energy source of this protein family, seems
643 to play only a regulatory role (9-13, 39). Moreover, in the case of LmrA, it remains
644 elusive whether this pump works as an importer or exporter. Besides these complex,
645 slightly contradicting studies, there are to our knowledge so far, no detailed
646 electrophysiological analysis of MDR ABC transporters *in vitro*. On basis of the
647 functionally purified, reconstituted Pdr5, and a well-studied ATPase deficient mutant as
648 a control as well as known substrates of Pdr5 (R6G, KA, CLO and CHX (15, 17, 18, 20,

649 40)) and the potent Pdr5-specific inhibitor BEA, we were able to perform an extensive
650 electrophysiological *in vitro* characterization of this MDR efflux pump.
651 In particular, we were able to demonstrate that $Pdr5_{WT}$, but not the ATPase-deficient
652 $Pdr5_{EQ}$ mutant, generated a membrane potential that can only be the result of a
653 substrate and Mg^{2+}-ATP driven proton co-transport across the membrane. These data
654 were also supported by *in vitro* measurements of bulk pH_{out} changes with Pdr5 enriched
655 plasma membrane vesicle suspensions. (Figure 9). Here, we observed an apparent
656 significant slower ATP hydrolysis driven decrease in ΔpH_{out} if the substrate, CLO, was
657 present. Considering that this time dependent decrease in $\Delta\Delta pH_{out}$ represents the rate
658 of H^+ cotransport into the vesicle lumen this results in an overall rate of $\tau \cong 22\ s^{-1}$ for
659 the H^+-co-transport mediated by Pdr5 within the suspension of yeast plasma membrane
660 vesicles.
661 This difference ($\Delta\Delta pH_{out}$) cannot be assigned to CLO induced alterations of the
662 ATPase activity of Pdr_{WT} as, the Pdr5–ATPase activity remained the same within
663 statistical error in the absence or presence of 1 µM CLO (Figure 9D). In contrast, Golin
664 *et al.* reported a slight stimulation of the ATPase activity of $Pdr5_{WT}$ in the presence of 1
665 µM CLO (41). Provided this would have been the case in our experiments, a stimulated
666 ATPase activity in the presence of the substrate would result in higher rates of released
667 H^+ due to the stimulated hydrolysis of ATP. This would result in an even larger
668 difference of the $\Delta\Delta pH_{out}$ decay-rate constant (Figure 9G). In summary our data
669 demonstrate that bulk pH_{out} changes with Pdr5 enriched plasma membrane vesicle
670 suspensions induced by the ATP-hydrolysis drop significantly in the presence of
671 substrate. We therefore conclude that Pdr5 is an ATP-dependent drug/H^+ co-
672 transporter that actively translocates substrates and generates an additional PMF
673 through vectorial proton efflux. Our electrophysiological measurements allowed not
674 only to prove that Pdr5 conducts ions and thereby follows the 'altered partitioning
675 model', but also to demonstrate that it actively transports its substrates across the
676 bilayer. Interestingly, the H^+ co-transport occurs independently of the charge of the
677 substrate and both, the cationic R6G as well as the neutral KA and CLO are transported
678 in a drug/H^+ co-transport fashion. The zero-current potentials for KA, CLO and R6G
679 (V_{rev} = – 64 ± 8 mV, -57.3 ± 6.7 mV and – 47.2 ± 5.3 mV, respectively) clearly show
680 that R6G is transported from cis to trans since due to the presence of R6G only on the
681 cis-side the putative V_{rev} of the $R6G^+$-ions contributes to the overall V_{rev}, reducing it in
682 comparison to the neutral KA and CLO. Additionally, using cationic and neutral

683 substrates, we demonstrate that the measured H^+ co-transport cannot be an artifact of
684 the efflux of a protonated or cationic substrate and instead is a real H^+ co-transport by
685 Pdr5 in a Mg^{2+}-ATP- and substrate-dependent manner. The recently described single
686 particle cryo-EM structures of Pdr5 (34) do not yet led to a direct identification of amino
687 acid residues potentially involved in protonation/deprotonation reactions leading to the
688 establishment of a vectorial H^+ translocation and finally the generation of an
689 electrochemical gradient $\Delta\bar{\mu}_{H^+}$. This situation is somehow reminiscent to LacY (42-44)
690 and further experiments are required to pin-point the molecular pathway of proton
691 transport.

692 The results presented in this study are also in line with the widely used R6G
693 transport assay that was established for Pdr5 located in inside-out oriented plasma
694 membrane vesicles (17, 18, 45, 46). R6G is a mitochondrial marker and a fluorescent
695 membrane potential probe (27). The observed fluorescence intensity decrease in
696 plasma membrane vesicles reflects the R6G and proton co-transport and thereby the
697 membrane potential change during transport.

698 Another tested substrate, CHX, however, did not induce any proton gradient or
699 change in conductance. In contrast to the majority of known Pdr5 substrates, CHX does
700 not affect the ATPase activity of Pdr5 and is hydrophilic (18, 20). One can speculate
701 that either a different transport route for this hydrophilic substrate exists, or that CHX is
702 not a substrate at all. The observed resistance conferred by Pdr5 could be due to
703 intracellular alkalization caused by Pdr5-mediated proton pumping as CHX undergoes
704 degradation at basic pH (47).

705 An interesting feature of Pdr5 is that it can be voltage activated thus allowing high
706 current fluxes across the membrane even in the absence of Mg^{2+}-ATP or substrates.
707 This activation occurred if Pdr5 was exposed to membrane voltages of V_h > +100 mV.
708 In a physiological context with a yeast plasma membrane potential of about -82 mV
709 (48) and an additional Pdr5 generated $\Delta\varphi$ of about $\Delta\varphi =$ -50 to -65 mV ($V_{rev, R6G}$ = –
710 47.2 ± 5.3 mV, $V_{rev, CLO}$ = -57.3 ± 6.7 mV, and $V_{rev, KA}$ = – 64 ± 8 mV), Pdr5 possibly
711 activates itself into this high conductance state.

712 Next to the self-activation, the proton pumping properties of Pdr5 with multiple
713 active copies would lead to the acidification in the trans compartment of our setup which
714 reflects an acidic external pH in an *in vivo* setting. Moreover, drug/proton co-transport
715 would temporarily significantly increase the membrane potential of the plasma
716 membrane thus effecting the ion and solute homeostasis and the membrane

717 morphology of yeast cells (49-51). This compares well with results that were obtained
718 previously for the Pdr5 homologue Cdr1 and MDR1 *in vivo* as it has been speculated
719 that MDR1 as well as Cdr1 may transport protons from the intra- to the extracellular
720 space and thus alkalize the cytoplasm (8, 38). However, the complexity of the cell
721 environment these *in vivo* experiments did not allow to unambiguously pinpoint
722 observations to a single protein level nor for the experimenter to control all relevant
723 critical cellular parameters. For Cdr1 it was hypothesized that the ABC transporter
724 creates an additional PMF when it was expressed in *S. cerevisiae*. In this context it is
725 important to note that in our experiments, the proton gradient does only occur in a
726 strictly Mg^{2+}-ATP and substrate dependent manner. This means that in the absence of
727 a substrate, Pdr5 does not participate in pH homeostasis of the membrane even if
728 ATPase activity is present. Therefore, the active proton pumping appears to be a
729 second mode of action of this MDR ABC transporter.

730 Furthermore, we demonstrate that Pdr5 conducts K^+ and Cl^- ions with a slight
731 cation selectivity. This is not surprising as all known charged substrates of Pdr5, like
732 for most other MDR ABC transporters, are cationic (15, 17, 37). We were also able to
733 show that the membrane part of the nucleotide-free Pdr5 switches between at least
734 three major confirmations as apparent from the three distinct subconductance states of
735 which the main state is compatible with a pore diameter of 6.4 Å (52), which is within
736 the range reported for other ABC transporters (53). Moreover, the broad distribution of
737 open channel states indicates that Pdr5 has a rather flexible membrane part
738 responsible for the translocation of its substrates. Additional experiments with the Pdr5
739 inhibitor BEA demonstrated that inhibition of the ATPase activity abolishes H^+-co-
740 transport and locks Pdr5 in an open conformation as indicated by the measured high
741 conductance. Molecular docking suggests that this is mediated via BEA binding to the
742 R6G binding site of Pdr5.

743 In conclusion, the presented data demonstrates that Pdr5 is an ATP-driven
744 drug/proton co-transporter that, unlike LmrA or MsbA, does not use the PMF but
745 creates a proton gradient across the membrane that results in self-activation and
746 presents a novel mechanism of drug resistance.
747
748

749 ## Materials and Methods

750

751 ### Pdr5 Expression and Purification

752 Pdr5 was expressed and purified as described (20). Briefly, *S. cerevisiae*
753 YRE1001 (18) cells were grown at 30 °C to a final OD_{600} of 3.5. Cells of 4 L YPD media
754 were harvested and disrupted using glass beads. Total membranes were collected
755 adjusted to 10 mg/ml total protein concentration with buffer A (50 mM Tris-HCl, pH 7.8,
756 50 mM NaCl, 10% (w/v) glycerol and solubilized for 1 h with 1% (w/v) trans-PCC-α-M
757 under gentle stirring at 4 °C. Immobilized metal ion affinity chromatography of the His-
758 tagged Pdr5 was performed with a Zn^{2+} loaded 1 ml HiTrap Chelating column (GE
759 Healthcare) and elution was carried out with a step gradient using low and high histidine
760 buffers (50 mM Tris-HCl pH 7.8, 500 mM NaCl, 10 % (w/v) glycerol, 0.003% (w/v) trans-
761 PCC-α-M and 2.5 mM or 100 mM L-histidine. The elution fractions were collected,
762 pooled and concentrated in a ultrafiltration unit (100 kDa MWCO). Size exclusion
763 chromatography was performed on a Superdex 200 10/300 GL column (GE
764 Healthcare) with buffer A containing 0.003 % (w/v) trans-PCC-α-M. All chromatography
765 steps were performed on Äkta protein purification systems (GE Healthcare).

766

767 ### Preparation of Pdr5 containing plasma membranes

768 Plasma membranes highly enriched in $Pdr5_{WT}$ were prepared as described in
769 (18).

770

771 ### Negative stain electron microscopy

772

773 4 µl sample droplets (plasma membranes sample enriched in Pdr5WT or Pdr5EQ) were
774 applied on freshly glow-discharged copper grids (Agar scientific; G2400C) covered by
775 a thin, continuous carbon film. The sample was left for 2min on the grid before blotting,
776 using filter paper (Whatman no. 4), subsequently washed with distilled water and
777 stained with 10 µl 0.75% uranyl formate. Images were taken with a Tecnai Spirit
778 electron microscope equipped with a LaB6 cathode operated at 120 kV. Digital electron
779 micrographs were recorded with a 4k x 4k CMOS camera F416 (TVIPS) at a
780 magnification of 67,000 x. (pixel size of 1.6 Å) using minimal dose conditions.

781

782

783

784 **Transport assays using Pdr5 containing plasma membranes**

785 Transport assays were performed according to the protocol developed by
786 Kolaczkowski and co-workers (17), using a FluoroLog III fluorescence spectrometer
787 (Horiba). Isolated plasma membranes (30 µg of total protein content) were
788 resuspended in 1 ml of transport buffer (50mM Hepes (pH 7.0), 10mM $MgCl_2$, 150 nM
789 R6G, and 10mM NaN_3) and incubated at 30 °C. R6G Transport was initiated by addition
790 of 5 mM ATP unless otherwise stated. The excitation wavelength was 529 nm (slit 1
791 nm) and the emission wavelength was 553 nm (slit 2 nm). For R6G transport data
792 shown in Figure 9, no Hepes buffer was added to the assay medium.

793

794 **Single Channel Recordings from Planar Lipid Bilayers and Data Analysis**

795 Planar lipid bilayer measurements using the Compact bilayer platform (Ionovation
796 GmbH) were performed as described in detail previously (54). In brief: if not explicitly
797 stated otherwise, symmetric conditions (250 mM KCl, 10 mM HEPES, pH 7.0) were
798 used in cis and trans compartments. The denomination cis and trans corresponds to
799 the half-chambers of the bilayer unit. Reported membrane potentials are always
800 referred to the trans compartment. Bilayer fabrication was performed on PFTE film at a
801 100 µm prepainted (1 % hexadecane in n-hexane) aperture with a Phosphatidylcholine
802 (18:1) (PC) / Phosphatidylethanolamine (18:1) (PE) (7:3 ratio) lipid mixture (both lipids
803 were purchased from Avanti Polar Lipids) in n-pentane using the “thinning method”
804 (54). Stock solutions of purified Pdr5 with typically 0.5-2.5 mg/ml contained in a buffer
805 of 50 mM Tris-HCl pH 7.8, 50 mM NaCl, and 0.003% (w/v) trans-PCC-α-M were added
806 to the cis compartment under slight stirring to a final protein concentration of ~1µg/ml
807 to 2µg/ml.

808 Ion channel currents were recorded using an EPC 10 USB amplifier (HEKA
809 Elektronik GmbH) in combination with the Patchmaster data acquisition software
810 (HEKA Elektronik GmbH). For data acquisition a sampling rate of 5kHz (voltage ramps)
811 and 10 kHz (continuous recording) was used and the data were further analyzed using
812 the Origin package (Origin Lab) and the MATLAB (MathWorks) based Ion-channel-
813 Master software developed in our laboratory (54).

814

815 **Molecular Docking**

816 For the molecular docking BEA was drawn and converted into 3D using the
817 ChemDraw19 suite. BEA was subsequently docked into four different Pdr5 cryo-EM
818 structures utilizing a combination of AutoDock as a docking engine and the
819 DrugScore2018 distance-dependent pair-potentials as an objective function. For this,
820 the co-resolved ligands were removed and the structures aligned on the R6G bound
821 Pdr5 structure using Pymol 2.4 (55). The DrugScore scoring grids were calculated for
822 each Pdr5 structure twice: It was centered on BEA, which was manually docked into
823 either the R6G binding site or the space between the TMDs and NBDs of Pdr5. Both
824 these initial BEA structures were docked into either grid to minimized starting structure
825 bias. During docking, default parameters were used, except for the clustering RMSD
826 cutoff, which was set to 2.0 Å(56-58). Binding modes were considered valid if they were
827 contained in the largest cluster with the most favorable docking energies, which
828 comprised at least 20 % of all docking poses.
829

830 **ATPase measurements in Pdr5-enriched plasma membranes**

831 Plasma membranes were prepared, and ATPase activity was determined as
832 described previously (18). Briefly, oligomycin (OM) sensitive ATPase activity of plasma
833 membrane fractions was measured by a colorimetric assay. Isolated plasma
834 membranes (0.2 µg per well) were incubated with 5 mM ATP, 5 mM $MgCl_2$ in 300 mM
835 Tris-glycine buffer (pH = 9.0) in a final volume of 100 µL. Pdr5-specific ATPase activity
836 was measured in presence or absence of 1 µM clotrimazole. To reduce background,
837 0.2 mM ammonium molybdate, 50 mM KNO_3, and 10 mM NaN_3 were added. In a
838 control reaction, OM (20 µg mL^{-1}) was added to the assay to determine the OM-
839 sensitive ATPase activity. After incubation at 30 °C for 20 min, the reaction was stopped
840 by adding 25 µL of the sample to 175 µL of ice-cold 40 mM H_2SO4. The amount of
841 released inorganic phosphate was determined by a colorimetric assay, using Na_2HPO_4
842 as standard.

843 **Fluorescence pH measurements**

844 pH measurements were performed accordingly to the R6G transport in Pdr5-
845 enriched plasma membranes, i.e. R6G was substituted by 2 µg/ml Fluorescein
846 conjugated Dextran (40,000 MW, see SI for further details). The excitation wavelength

847 was 494 nm (slit width 1 nm) and the emission wavelength was 521 nm (slit width 2
848 nm). The pH measurements were performed in absence or presence of 1 µM
849 clotrimazole. For data evaluation a calibration curve with a R-squared value of 0.94
850 was generated using 50 mM KP_i buffer with defined pH values between 6.5 and 8.0.

851

852 ## Acknowledgments

853 We thank Prof. Oliver Ebenhöh (Heinrich Heine University Düsseldorf), Prof. Alexej
854 Kedrov and all members of the Institute of Biochemistry for stimulating discussions. We
855 also thank Prof. Mathias Winterhalter (Jacobs University Bremen) for support. A.S.-H.
856 was funded through ERC Advanced grant VisTrans (ID: 742210). The Center for
857 Structural Studies is funded by the Deutsche Forschungsgemeinschaft (DFG Grant
858 number 417919780 to S.S.).

859

860 ## Acknowledgments

861 The authors declare no financial and non-financial competing interest.

862 ## References

863

864 1. Gottesman MM, Fojo T, & Bates SE (2002) Multidrug resistance in cancer: role
865 of ATP-dependent transporters. *Nat Rev Cancer* 2:48-58.

866 2. Sa-Correia I, dos Santos SC, Teixeira MC, Cabrito TR, & Mira NP (2009)
867 Drug:H+ antiporters in chemical stress response in yeast. *Trends Microbiol*
868 17:22-31.

869 3. Kumar S*, et al.* (2016) Bacterial Multidrug Efflux Pumps of the Major Facilitator
870 Superfamily as Targets for Modulation. *Infect Disord Drug Targets* 16:28-43.

871 4. Quistgaard EM, Low C, Guettou F, & Nordlund P (2016) Understanding
872 transport by the major facilitator superfamily (MFS): structures pave the way.
873 *Nature reviews. Molecular cell biology* 17:123-132.

874 5. Schmitt L & Tampe R (2002) Structure and mechanism of ABC transporters.
875 *Curr Opin Struct Biol* 12:754-760.

876 6. Chang G (2003) Multidrug resistance ABC transporters. *FEBS letters* 555:102-
877 105.

878 7. Roepe P (2000) What is the Precise Role of Human MDR 1 Protein in
879 Chemotherapeutic Drug Resistance. *Curr Pharm Des* 6:241-260.

880 8. Milewski S, Mignini F, Prasad R, & Borowski E (2001) Unusual susceptibility of
881 a multidrug-resistant yeast strain to peptidic antifungals. *Antimicrobial agents*
882 *and chemotherapy* 45:223-228.

883 9. Venter H, Shilling RA, Velamakanni S, Balakrishnan L, & van Veen HW (2003)
884 An ABC transporter with a secondary-active multidrug translocator domain.
885 *Nature* 426:866-870.

886 10. van den Berg van Saparoea HB, Lubelski J, van Merkerk R, Mazurkiewicz PS,
887 & Driessen AJ (2005) Proton motive force-dependent Hoechst 33342 transport
888 by the ABC transporter LmrA of Lactococcus lactis. *Biochemistry* 44:16931-
889 16938.

890 11. Velamakanni S*, et al.* (2009) A multidrug ABC transporter with a taste for salt.
891 *PloS one* 4:e6137.

892 12. Agboh K*, et al.* (2018) Powering the ABC multidrug exporter LmrA: How
893 nucleotides embrace the ion-motive force. *Science advances* 4.

894 13. Singh H*, et al.* (2016) ATP-dependent substrate transport by the ABC
895 transporter MsbA is proton-coupled. *Nature communications* 7:12387.

896 14. Balzi E, Wang M, Leterme S, Van Dyck L, & Goffeau A (1994) PDR5, a novel
897 yeast multidrug resistance conferring transporter controlled by the transcription
898 regulator PDR1. *J Biol Chem* 269:2206-2214.

899 15. Rogers B*, et al.* (2001) The pleitropic drug ABC transporters from
900 Saccharomyces cerevisiae. *Journal of molecular microbiology and*
901 *biotechnology* 3:207-214.

902 16. Golin J & Ambudkar SV (2015) The multidrug transporter Pdr5 on the 25th
903 anniversary of its discovery: an important model for the study of asymmetric
904 ABC transporters. *Biochem J* 467:353-363.

905 17. Kolaczkowski M*, et al.* (1996) Anticancer Drugs, Ionophoric Peptides, and
906 Steroids as Substrates of the Yeast Multidrug Transporter Pdr5p. *Journal of*
907 *Biological Chemistry* 271:31543-31548.

908 18. Ernst R*, et al.* (2008) A mutation of the H-loop selectively affects rhodamine
909 transport by the yeast multidrug ABC transporter Pdr5. *Proc Natl Acad Sci U S*
910 *A* 105:5069-5074.

911 19. Mamnun YM, Schuller C, & Kuchler K (2004) Expression regulation of the
912 yeast PDR5 ATP-binding cassette (ABC) transporter suggests a role in cellular
913 detoxification during the exponential growth phase. *FEBS letters* 559:111-117.

914 20. Wagner M, Smits SHJ, & Schmitt L (2019) In vitro NTPase activity of highly
915 purified Pdr5, a major yeast ABC multidrug transporter. *Scientific reports*
916 9:7761.

917 21. Arbeloa FL, Ojeda PR, & Arbeloa IL (1988) Dimerization and Trimerization of
918 Rhodamine 6g in Aqueous-Solution - Effect on the Fluorescence Quantum
919 Yield. *J Chem Soc Farad T 2* 84:1903-1912.

920 22. Kang PT, Chen CL, Lin P, Chilian WM, & Chen YR (2017) Impairment of pH
921 gradient and membrane potential mediates redox dysfunction in the
922 mitochondria of the post-ischemic heart. *Basic Res Cardiol* 112:36.

923 23. Selivanov VA*, et al.* (2008) The role of external and matrix pH in mitochondrial
924 reactive oxygen species generation. *J Biol Chem* 283:29292-29300.

925 24. Ho L-C*, et al.* (2013) Sensitive pH probes of retro-self-quenching fluorescent
926 nanoparticles. *Journal of Materials Chemistry B* 1:2425-2432.

927 25. Aiuchi T, Daimatsu T, Nakaya K, & Nakamura Y (1982) Fluorescence changes
928 of rhodamine 6G associated with changes in membrane potential in
929 synaptosomes. *Biochim Biophys Acta* 685:289-296.

930 26. Aiuchi T, Tanabe H, Kurihara K, & Kobatake Y (1980) Fluorescence changes
931 of rhodamine 6G associated with chemotactic responses in Tetrahymena
932 pyriformis. *Biochim Biophys Acta* 628:355-364.

933 27. Mandala M, Serck-Hanssen G, Martino G, & Helle KB (1999) The fluorescent
934 cationic dye rhodamine 6G as a probe for membrane potential in bovine aortic
935 endothelial cells. *Anal Biochem* 274:1-6.

936 28. Hille B (1968) Pharmacological modifications of the sodium channels of frog
937 nerve. *The Journal of general physiology* 51:199-219.

938 29. Smart OS, Breed J, Smith GR, & Sansom MS (1997) A novel method for
939 structure-based prediction of ion channel conductance properties. *Biophys J*
940 72:1109-1126.

941 30. Bartsch P, Harsman A, & Wagner R (2013) Single channel analysis of
942 membrane proteins in artificial bilayer membranes. *Membrane Biogenesis:*
943 *Methods and Protocols*:345-361.

944 31. Goldman E (1943) Potentials impedance, and rectification in membranes. *The*
945 *Journal of general physiology* 27:37-60.

946 32. Shekhar-Guturja T*, et al.* (2016) Dual action antifungal small molecule
947 modulates multidrug efflux and TOR signaling. *Nature chemical biology*
948 12:867-875.

949 33. Benz R (1978) Alkali ion transport through lipid bilayer membranes mediated
950 by enniatin A and B and beauvericin. *J Membr Biol* 43:367-394.

951 34. Harris A*, et al.* (2021) Structure and efflux mechanism of the yeast pleiotropic
952 drug resistance transporter Pdr5. *Nature communications* 12:5254.

953 35. Plewczynski D, Łaźniewski M, Augustyniak R, & Ginalski K (2011) Can we
954 trust docking results? Evaluation of seven commonly used programs on
955 PDBbind database. *J. Comput. Chem.* 32:742-755.

956 36. Sharom FJ (1997) The P-Glycoprotein Efflux Pump: How Does it Transport
957 Drugs? *J Membr Biol* 160:161-175.

958 37. Ambudkar SV*, et al.* (1999) Biochemical, cellular, and pharmacological aspects
959 of the multidrug transporter. *Annual review of pharmacology and toxicology*
960 39:361-398.

961 38. Hoffman MM & Roepe PD (1997) Analysis of ion transport perturbations
962 caused by hu MDR 1 protein overexpression. *Biochemistry* 36:11153-11168.

963 39. Velamakanni S, Yao Y, Gutmann DA, & van Veen HW (2008) Multidrug
964 transport by the ABC transporter Sav1866 from Staphylococcus aureus.
965 *Biochemistry* 47:9300-9308.

966 40. Arya N*, et al.* (2019) An A666G mutation in transmembrane helix 5 of the yeast
967 multidrug transporter Pdr5 increases drug efflux by enhancing cooperativity
968 between transport sites. *Molecular microbiology* 112:1131-1144.

969 41. Golin J*, et al.* (2007) Complete inhibition of the Pdr5p multidrug efflux pump
970 ATPase activity by its transport substrate clotrimazole suggests that GTP as
971 well as ATP may be used as an energy source. *Biochemistry* 46:13109-13119.

972 42. Bazzone A, Madej MG, Kaback HR, & Fendler K (2016) pH Regulation of
973 Electrogenic Sugar/H+ Symport in MFS Sugar Permeases. *PloS one*
974 11:e0156392.

975 43. Kaback HR (2015) A chemiosmotic mechanism of symport. *Proc Natl Acad Sci*
976 *U S A* 112:1259-1264.

977 44. Smirnova I, Kasho V, Sugihara J, Choe JY, & Kaback HR (2009) Residues in
978 the H+ translocation site define the pKa for sugar binding to LacY.
979 *Biochemistry* 48:8852-8860.

980 45. Gupta RP, Kueppers P, Hanekop N, & Schmitt L (2014) Generating symmetry
981 in the asymmetric ATP-binding cassette (ABC) transporter Pdr5 from
982 Saccharomyces cerevisiae. *J Biol Chem* 289:15272-15279.

983 46. Furman C*, et al.* (2013) The deviant ATP-binding site of the multidrug efflux
984 pump Pdr5 plays an active role in the transport cycle. *J Biol Chem* 288:30420-
985 30431.

986 47. Garrett ER & Notari RE (1965) Cycolheximide Transformations. Ii. Kinetics and
987 Stability in a Pharmaceutically Useful Ph Range. *Journal of pharmaceutical*
988 *sciences* 54:209-215.

989 48. Borst-Pauwels GWFH (1981) Ion Transport in yeast. *Biochimica et Biophysica*
990 *Acta (BBA) - Reviews on Biomembranes* 650:88-127.

991 49. Grossmann G, Opekarova M, Malinsky J, Weig-Meckl I, & Tanner W (2007)
992 Membrane potential governs lateral segregation of plasma membrane proteins
993 and lipids in yeast. *The EMBO journal* 26:1-8.

994 50. Vacata V, Kotyk A, & Sigler K (1981) Membrane potential in yeast cells
995 measured by direct and indirect methods. *Biochimica et Biophysica Acta*
996 *(BBA)-Biomembranes* 643:265-268.

997 51. Kinclova-Zimmermannova O, Gaskova D, & Sychrova H (2006) The Na+,
998 K+/H+-antiporter Nha1 influences the plasma membrane potential of
999 Saccharomyces cerevisiae. *FEMS yeast research* 6:792-800.

1000 52. Corry B, Kuyucak S, & Chung S-H (2000) Tests of continuum theories as
1001 models of ion channels. II. Poisson–Nernst–Planck theory versus Brownian
1002 dynamics. *Biophys J* 78:2364-2381.

1003 53. Bi Y, Mann E, Whitfield C, & Zimmer J (2018) Architecture of a channel-
1004 forming O-antigen polysaccharide ABC transporter. *Nature* 553:361-365.

1005 54. Bartsch P, Harsman A, & Wagner R (2013) Single channel analysis of
1006 membrane proteins in artificial bilayer membranes. *Methods in molecular*
1007 *biology* 1033:345-361.

1008 55. DeLano WL (2002) Pymol: An open-source molecular graphics tool. *CCP4*
1009 *Newsletter on protein crystallography* 40:82-92.

1010 56. Goodsell DS, Morris GM, & Olson AJ (1996) Automated docking of flexible
1011 ligands: applications of AutoDock. *J. Mol. Recognit.* 9:1-5.

1012 57. Sotriffer CA, Gohlke H, & Klebe G (2002) Docking into knowledge-based
1013 potential fields: a comparative evaluation of DrugScore. *J. Med. Chem.*
1014 45:1967-1970.

1015 58. Dittrich J, Schmidt D, Pfleger C, & Gohlke H (2019) Converging a Knowledge-
1016 Based Scoring Function: DrugScore2018. *J. Chem. Inf. Model.*

1017